Effects of lower troposphere vertical mixing on simulated clouds and precipitation over the Amazon during the wet season

Xiao-Ming Hu[1,2], Yongjie Huang[1], Ming Xue[1,2], Elinor Martin[2], Yang Hong[3], Mengye Chen[3], Hector Mayol Novoa[4], Renee McPherson[5], Andres Perez[4], Isaac Yanqui Morales[4], Auria Julieta Flores Luna[4]

[1] Center for Analysis and Prediction of Storms, University of Oklahoma, Norman, Oklahoma, 73072, USA
[2] School of Meteorology, University of Oklahoma, Norman, Oklahoma, 73072, USA
[3] School of Civil Engineering and Environmental Engineering, University of Oklahoma, Norman, Oklahoma, 73072, USA
[4] Universidad Nacional de San Agustín de Arequipa, Arequipa, Perú
[5] Department of Geography and Environmental Sustainability, University of Oklahoma, Norman, Oklahoma, 73072, USA

Submitted to

Journal of Geophysical Research-Atmospheres

on 1/19/2023 3:47 PM

Corresponding author address:
Drs. Xiao-Ming Hu (xhu@ou.edu), Ming Xue (mxue@ou.edu)
Hector Mayol Novoa (hnovoa@unsa.edu.pe),
Phone: (405) 325- 0402
Center for Analysis and Prediction of Storms, and School of Meteorology
University of Oklahoma
Norman, Oklahoma 73072, USA

Key points: (≤140 characters)

1. disentangle the turbulence/cloud/precipitation processes over Amazon and reveal root causes for precipitation sensitivity to PBL schemes.
2. FT mixing becomes prominent in the presence of clouds, which in turn supports maintenance of the FT clouds that would otherwise dissipate.
3. Stronger vertical moisture relay transport in ACM2 PBL scheme supports thicker FT clouds, leading to reduced heating and precipitation.

Abstract

Planetary boundary layer (PBL) schemes parameterize unresolved turbulent mixing within the PBL and free troposphere (FT). Previous studies reported that precipitation simulation over the Amazon in South America is quite sensitive to PBL schemes and the exact relationship between the turbulent mixing and precipitation processes is, however, not disentangled. In this study, regional climate simulations over the Amazon in January-February 2019 are examined at process level to understand the precipitation sensitivity to PBL scheme. The focus is on two PBL schemes, the Yonsei University (YSU) scheme, and the asymmetric convective model v2 (ACM2) scheme, which show the largest difference in the simulated precipitation. During daytime, while the FT clouds simulated by YSU dissipate, clouds simulated by ACM2 maintain because of enhanced moisture supply due to the enhanced vertical moisture relay transport process: 1) vertical mixing within PBL transports surface moisture to the PBL top, and 2) FT mixing feeds the moisture into the FT cloud deck. Due to the thick cloud deck over Amazon simulated by ACM2, surface radiative heating is reduced and consequently the convective available potential energy (CAPE) is reduced. As a result, precipitation is weaker from ACM2. Two key parameters dictating the vertical mixing are identified, p, an exponent determining boundary layer mixing and λ, a scale dictating FT mixing. Sensitivity simulations with altered p, λ, and other treatments within YSU and ACM2 confirm the precipitation sensitivity. The FT mixing in the presence of clouds appears most critical to explain the sensitivity between YSU and ACM2.

Plain Language Summary (≤200 words)

Predictions of weather and climate in terms of clouds and precipitation over the Amazon in South America are quite uncertain. This uncertainty has been largely attributed to errors in the planetary boundary layer (PBL) scheme, which represents turbulent mixing. A lack of understanding of the relationship between turbulence, clouds, and precipitation processes prevents us from improving PBL representation in models to achieve better weather and climate simulations.

This study disentangles the turbulence/clouds/precipitation relationship, and identifies the root cause of model errors in PBL schemes using regional climate simulations over the Amazon. Two PBL schemes, the Yonsei University (YSU) scheme, and the asymmetric convective model v2 (ACM2) scheme, are examined, which show the largest difference in the simulated precipitation.

The main difference between the two PBL schemes is the dissipation (YSU) or maintenance (ACM2) of clouds during daytime above the boundary layer, which modulates surface heating and consequently precipitation. The maintenance of a thick cloud deck over the Amazon in ACM2, is caused by enhanced vertical transport of moisture from the surface to above the boundary layer. Such an improved understanding of the turbulence/clouds/precipitation relationship allow us to propose potential solutions to improve PBL schemes in weather and climate models

Keywords: Clouds, precipitation, free troposphere vertical mixing, regional climate dynamical downscaling

1. Introduction

Climate change can cause shifted weather patterns, more extreme weather events, reduced water availability, change in agricultural patterns and increased exposure to disease (Langenbrunner et al., 2019; Prein et al., 2017; Vera et al., 2006) and other significant impacts on society. Accurate simulation of regional climate and the development of adaptation strategies and corresponding policies are critical. Global climate model (GCM) simulations are too coarse to resolve local forcing and local weather, and their precipitation simulation is generally poor. Cloud-resolving regional climate model (RCM) simulations have emerged in recent years for dynamically downscaling global climate simulations and climate change responses at spatial scales that are more useful for decision making (Huang et al., 2022; Liu et al., 2022; Prein et al., 2022; Prein et al., 2015; Prein et al., 2017; Sun et al., 2016). However, compared to mid-latitude regions, the performance of RCM simulations in reproducing precipitation over tropical regions, such as the Amazon in South America, is understudied (Chakraborty et al., 2020; Prein et al., 2022; Tai et al., 2021).

Noontime and afternoon mesoscale convective systems (MCSs) are the main source of precipitation over the Amazon and thus Amazonian precipitation has a single afternoon peak in diurnal cycle (Giangrande et al., 2017; Giangrande et al., 2020; Prein et al., 2022; Wu et al., 2021a). Moist advection from the Atlantic Ocean by northeasterly trade winds during the austral summer wet season (January - February) and zonal wind convergence are important for precipitation over the Amazon rainforest (Fu et al., 1999) and cloud and turbulence processes play critical roles in modulating precipitation in the region (Barber et al., 2022; Chakraborty et al., 2020; Chakraborty et al., 2018; Prein et al., 2022; Wright et al., 2017). The relationship between processes of clouds, turbulence, and precipitation in the region remains to be disentangled and their modelling uncertainties and sensitivities need to be understood to improve simulations (Giangrande et al., 2017; Giangrande et al., 2020; Prein et al., 2022).

Simulated precipitation over the Amazon is sensitive to the planetary boundary layer (PBL) scheme, but the root cause for such sensitivity and the cause-effect relationship remain to be disentangled (Prein et al., 2022). Within typical weather and climate models, PBL schemes parameterize unresolved turbulent mixing within the PBL and the free troposphere; the PBL schemes are therefore critical for reproducing the bulk boundary layer structures and profiles in the whole atmospheric column, as well as their subsequent effects on weather and climate

simulations. Many studies (Gunwani & Mohan, 2017; Hu et al., 2012; Hu et al., 2013a; Hu et al., 2010a; Hu et al., 2019; Wang & Hu, 2021) have evaluated the performance of various modern PBL schemes, with most of them focusing on continental cloud-free PBL. Compared to continental clear PBL, much less is known about the performance of PBL schemes in presence of clouds (Angevine et al., 2012; Huang et al., 2013; Supinie et al., 2022; Yang et al., 2019).

PBL schemes can be classified into local and nonlocal schemes. Local schemes estimate the turbulent fluxes at each point in a model from the mean atmospheric variables and/or their gradients at that point, whereas nonlocal schemes include turbulent fluxes based on the atmospheric variables and their variations over a deeper layer covering multiple model levels through the PBL (Cohen et al., 2015; Hu et al., 2010a). The assumption among local schemes that fluxes depend solely on local values and local gradients of model state variables is least valid under convective conditions when turbulent fluxes are dominated by large eddies that transport fluid over longer distances (Hu et al., 2010a). Previous studies found that traditional local schemes (e.g., Mellor–Yamada–Janjić (MYJ) or quasi-normal scale elimination (QNSE)) predict daytime continental boundary layers that are too cool and shallow; while schemes that include non-local treatment, such as the Asymmetrical convective model, version 2 (ACM2, Pleim, 2007), the Yonsei University (YSU, Hong et al., 2006) schemes and the more recently-updated local scheme (e.g., Mellor–Yamada Nakanishi and Niino (MYNN, Nakanishi & Niino, 2006)) predict deeper and warmer daytime continental boundary layers than MYJ and QNSE (Bright & Mullen, 2002; Clark et al., 2015; Coniglio et al., 2013). Also, nonlocal PBL schemes can reproduce the slightly stable upper convective boundary layer while local schemes often fail to do so (Hu et al., 2019; Wang et al., 2016).

Recent PBL development has started to use the mass flux (MF) approach that has been commonly used in cumulus parameterization schemes for large-eddy nonlocal mixing together with the eddy-diffusivity (ED) closure parameterizing local mixing, such as the MYNN-EDMF scheme (Angevine et al., 2010; Olson et al., 2019a; Olson et al., 2019b; Pergaud et al., 2009). Most previous PBL modeling studies focus on treatments within the boundary layer while free-troposphere treatments rarely receive much attention (Hu et al., 2012; Lu & Wang, 2019; Zhu et al., 2021; Zhu et al., 2019), likely because that free-troposphere turbulence is weak under clear conditions and the impact of its parameterization on weather and climate simulations is regarded as minor.

Huang et al. (2022) conducted nested-domain RCM simulations with grid spacings of 15 and 3 km over the Amazon with different physics schemes. It is found that the simulated precipitation is most sensitive to PBL schemes with the YSU scheme significantly overpredicting Amazonian precipitation and the ACM2 scheme predicting the weakest precipitation. Extending the work of Huang et al. (2022), this study aims to understand the precipitation sensitivity over the Amazon at a process level and identify the root cause for the different model behaviors, with particular attention paid to the behaviors and effects of PBL schemes in cloudy environments, and both inside and above the PBL. Effects of lower troposphere vertical mixing on simulated clouds and precipitation over the Amazon will be elucidated.

The rest of this paper is organized as follows: In section 2, precipitation data, model configurations, and numerical experiment design are described. In section 3, clouds/precipitation sensitivity to PBL schemes is diagnosed using simulations with YSU and ACM2 and their variants with altered turbulence treatments, followed by discussion of such sensitivity at a finer resolution. Meanwhile the turbulence/cloud/precipitation processes over the Amazon are examined. Finally, section 4 contains a summary and discussion of the main findings.

2. Precipitation data, model configuration and numerical experiment design

a) Precipitation data

Two gridded global precipitation datasets are used in this study to compare with simulations, including (1) half-hourly Integrated Multi-satellitE Retrievals for GPM (IMERG) at a horizontal resolution of 0.1° × 0.1° (Huffman et al., 2019), and (2) half-hourly National Oceanic and Atmospheric Administration (NOAA) Climate Prediction Center (CPC) MORPHing Technique (CMORPH) global precipitation analyses at a horizontal resolution of ~8 km (Joyce et al., 2004).

b) Model configurations

Huang et al. (2022) used the Weather Research and Forecasting (WRF) model Version 4.2.1 (Skamarock & Klemp, 2008; Skamarock et al., 2021) to perform historical simulations over South America during January-February 2019 in preparation for future regional climate dynamic downscaling. The simulations used hourly European Centre for Medium-Range Weather Forecasts Reanalysis v5 (ERA5, Hersbach et al., 2020) for initial and boundary conditions. Two one-way

nested domains with 15- and 3-km horizontal grid spacings cover the entire South America and the Peruvian central Andes region, respectively (see Fig. 1a for domain coverage). Both domains use 61 stretched vertical levels topped at 20 hPa. Following previous dynamic downscaling practices (Hu et al., 2018; Miguez-Macho et al., 2004, 2005; Wang & Kotamarthi, 2013), spectral nudging technique is applied to the outer 15-km domain to maintain large-scale circulations at a 1500 km scale, while allowing WRF to evolve smaller-scale dynamics and physics. Twelve sensitivity experiments were conducted by Huang et al. (2022) with varied PBL, microphysics schemes, and land surface models while other physics parameterizations were kept the same among the sensitivity experiments, including revised MM5 Monin-Obukhov surface layer scheme (Jiménez et al., 2012), and the Rapid Radiative Transfer Model for GCMs (RRTMG) longwave and shortwave radiation scheme (Iacono et al., 2008). The Tiedtke cumulus parameterization scheme (Tiedtke, 1989) is used on the 15-km outer domain but not on the 3-km inner domain.

These WRF downscaling simulations are found to be most sensitive to PBL schemes with the YSU scheme significantly overpredicting Amazonian precipitation, the ACM2 scheme predicting the weakest precipitation, and the MYNN-EDMF prediction being in the middle. Such relative differences are maintained with altered microphysics schemes and land surface models (LSMs). Simulations with the Thompson microphysics scheme (Thompson et al., 2008), and the Noah LSM (Chen & Zhang, 2009) are chosen to investigate PBL sensitivities in this study. Diagnosing the root cause for the differences between the YSU and ACM2 PBL schemes and disentangle the impact of PBL schemes on precipitation are the foci of this study. Since simulated precipitation is quite sensitive to some other parameterization, such as cumulus schemes (Hu et al., 2018), and there are large uncertainties among different precipitation data (Chen et al., 2022), recommending an optimal PBL scheme in terms of reproducing precipitation is beyond the scope of this study, which may require more advanced profile measurements (e.g., cloud water profile) and more accurate precipitation data to justify as will be seen in our later analyses.

c) Sensitivity simulations with altered treatments in ACM2 and YSU

In addition to the simulations conducted by Huang et al. (2022), eight more sensitivity simulations (summarized in Table 1) are run to help identify the root cause of the differences between ACM2 and YSU, and resolution dependence of the differences, as well as to examine impact of turbulent processes on cloud and precipitation processes. ACM2 and YSU differ in their

206 treatments in both PBL and free troposphere. Sensitivity simulations adjusting either PBL or free-
207 troposphere mixing treatments or both are conducted.

208 In the PBL, while a counter-gradient term is added to the eddy diffusion equation to handle
209 nonlocal mixing in YSU, ACM2 explicitly simulates the transilient nonlocal mass flux. For the
210 local mixing in the PBL, both ACM2 and YSU use a polynomial function/profile (so called K-
211 profile, Noh et al., 2003) to define the vertical mixing coefficient K_z as:

212 $$K_z = k\frac{u_*}{\emptyset}z(1-\frac{z}{h})^p \qquad (1)$$

213 where k is the von Karman constant, ϕ is the similarity profile function, z is the height above ground
214 level, and h is the PBL height. Thus, ACM2 and YSU are also categorized into the *K*-profile PBL
215 schemes (Hu et al., 2019). In YSU and ACM2, the value of the exponent p in (1) is 2, but it may
216 vary from 0.5 to 3 depending on flow conditions, with a larger/smaller p yielding smaller/larger
217 K_z (Hu et al., 2018; Hu et al., 2010b; Nielsen-Gammon et al., 2010; Troen & Mahrt, 1986). While
218 a similar local mixing treatment is adopted in ACM2 and YSU, there are many differences in their
219 parameter values, profile functions, methods to diagnose PBL height, etc. ACM2 generally
220 simulates stronger vertical mixing in the PBL and higher PBL height under clear conditions (Hu
221 et al., 2010a). Since p effectively dictates the vertical mixing within the PBL, p is varied in
222 sensitivity simulations to understand model differences and physics processes including turbulence,
223 clouds, and precipitation.

224 In the free troposphere, both YSU and ACM2 compute the K_z as a function of mixing
225 length l, vertical wind shear S, and the stability function $f(Ri)$:

226 $$K_z = l^2 S f(Ri)\ , \qquad (2)$$

227 in which

228 $$\frac{1}{l} = \frac{1}{kz} + \frac{1}{\lambda}\ , \qquad (3)$$

229 where Ri is the Richardson number, and λ is the asymptotic length scale. Such first-order
230 parameterizations of turbulent vertical mixing are widely used in operational numerical weather
231 prediction (NWP) and climate models (Beare et al., 2006; Cuxart et al., 2006). ACM2 and YSU
232 differ in their parameter values, Ri calculation within clouds, and stability functions. Both ACM2

and YSU use moist-air Ri calculation adapted from Durran and Klemp (1982), but YSU requires two layers of clouds to activate the moist-air Ri calculation between the two layers while ACM2 only requires one layer, in addition to other differences in parameters. Much of the improvement to such parameterizations (Eqs. 2-3) in NWP and climate models involved adjusting the stability functions (for example short vs. long-tailed functions) and λ (Cuxart et al., 2006). λ is adjustable and varies between 30 and 250 m in numerical models (Cuxart et al., 2006; Liu & Carroll, 1996; Nielsen-Gammon et al., 2010). λ is set to 30 m in the YSU scheme and to 80 m in the ACM2 scheme. Sensitivity simulations are conducted in this study by replacing the whole free-troposphere treatments or only altering the value of λ.

The sensitivity simulations are conducted with the outer 15 km domain because the difference between inner-domain outputs from our nested-domain runs with different configurations are rooted from the different simulations in the outer 15km domain, as we will see in our analysis. Thus, the conclusions from these sensitivity simulations have implications for regional and global models that run at convection-parameterized resolutions. In addition, four sensitivity simulations with a single domain covering the majority of the Amazon with a 3 km grid spacing are also conducted to examine the applicability of conclusions obtained at 15 km grid spacing to convection-allowing simulations.

3. Results

a) Cause of precipitation differences simulated with different PBL schemes

As stated earlier, WRF simulations over South America during January-February 2019 are conducted with 12 different physics schemes, including PBL, microphysics schemes and land surface models (Huang et al., 2022). The simulated precipitation is most sensitive to PBL schemes (Huang et al., 2022) with the YSU scheme predicting the strongest daily precipitation rate while the ACM2 scheme predicting the weakest precipitation over the Amazon during the summer wet season (Fig. 1). The relative strength of simulated precipitation between ACM2 and YSU remains across different resolutions, including the convection-parameterized (15 km grid spacing) and convection-permitting (3 km grid spacing) resolutions. The precipitation rate increases with increased resolution. The YSU runs at 3 km grid spacing (including the nested run focusing on Peru and the single-domain run focusing more on the Amazon) significantly overestimate daily

precipitation rate (Figs. 1c-f). The South America Affinity Group (SAAG) led by National Center for Atmospheric Research (NCAR) also reported that a WRF simulation using the YSU scheme at a grid spacing of 4 km over South America overestimated precipitation over the Amazon (Liu et al., 2022).

Precipitation over the Amazon is dominated by mid-day and afternoon MCSs (Giangrande et al., 2017; Giangrande et al., 2020; Prein et al., 2022; Wu et al., 2021a). Thus, we will focus on the precipitation and related processes during daytime. During mid-day hours, YSU simulates stronger hourly precipitation rates than ACM2 and overestimates precipitation at both resolutions and over different domains (Fig. 2).

Causative factors for the different precipitation simulated by ACM2 and YSU over the Amazon are herein investigated. The impact of different PBL schemes on NWP and climate simulations is more straightforward under clear conditions while their impacts on precipitation is less clear. Often the impact of PBL schemes on precipitation is not conclusive because the schemes produce different (stronger or weaker) precipitation in different cases (Bright & Mullen, 2002; Cohen et al., 2015; Jankov et al., 2005; Jankov et al., 2007; Li & Pu, 2008; Supinie et al., 2022; Wu et al., 2021b; Zhang et al., 2013). Under clear conditions, ACM2 simulates stronger boundary layer vertical mixing and deeper PBL than YSU due to different treatments for nonlocal fluxes and different parameters/functions in the *K*-profile local mixing (Hu et al., 2010a; Nielsen-Gammon et al., 2010; Shin & Hong, 2011; Xie et al., 2012). How such differences translate to significantly different precipitation with the two schemes is the main question to be answered in this study.

Surface temperature shows distinct differences over the Amazon with the ACM2 simulating lower continental temperatures than YSU by 0.5-0.8 ^{o}C over the simulation domains around noon (Fig. 3), which likely leads to less surface energy to feed MCSs. The lower temperature simulated by ACM2 covers the main precipitation region over the Amazon (Fig. 3g) and can likely explain the precipitation difference. However, such temperature differences cannot be explained by the direct impact of PBL mixing. Prior work has shown that during daytime, ACM2 simulates stronger mixing in the PBL and stronger PBL-free troposphere exchange generally warming up the PBL due to entrainment of free troposphere air with higher potential temperature (Hu et al., 2010a; Shin & Hong, 2011). Thus, the direct impact of ACM2 PBL mixing

should lead to higher surface temperature, rather than the lower temperature obtained in the regions of precipitation.

Rather, the temperature difference between ACM2 and YSU simulations is more directly related to the difference in surface downward shortwave radiation. ACM2 simulates less shortwave radiation at the surface over the Amazon region (Fig. 4g), where cloud coverage is significant (Fig. 4j). At 17 UTC (12-14 LST across south America), the average surface shortwave radiation simulated by ACM2 is lower by ~70 W m^{-2} than the YSU runs. Thus, the lower temperature simulated by ACM2 should be due to indirect effects of vertical mixing via interactions with clouds and radiation.

Significant cloud coverage over the Amazon (Kay et al., 2016; Kay et al., 2012) is a characteristic distinguishing this study from most other studies of PBL schemes. Over the Amazonian region, ACM2 simulates a thicker cloud deck (Fig. 5,6), which reduces downward shortwave radiation (Fig. 7), consequently leading to a lower surface temperature. As a result, the surface-based convective available potential energy (CAPE) is lower in the ACM2 simulations (Fig. 8), which would lead to weaker daytime precipitation. The significant difference between YSU and ACM2 is mostly confined over the cloud region (Fig. 4 & 7), which further confirms that indirect effects of vertical mixing over the Amazon via interactions with clouds dominates its direct effects.

The cloud deck over the Amazon therefore appears to be a critical link to disentangle the impact of PBL schemes on simulated precipitation. During daytime, while the clouds simulated with the YSU scheme dissipate gradually from the early morning maxima, clouds simulated with the ACM2 scheme are still sustained through the day (see cloud cross-sections at 11 - 21 UTC in Fig. 5). Daytime cloud thinning is likely due to solar heating under condition of lack of water vapor supply available for condensation (Adebiyi et al., 2020; Burleyson & Yuter, 2015; Painemal et al., 2015; Zhang et al., 2010). The thicker cloud deck simulated by ACM2 appears to be due to enhanced supply of boundary layer moisture to the layers above (thus less boundary layer moisture by 0.6 g kg^{-1} and more free troposphere moisture by 0.2 g kg^{-1} compared to the YSU run, Fig. 9b), through enhanced boundary layer vertical mixing (Hu et al., 2010a; Shin & Hong, 2011).

In the nested-domain simulations, surface temperature simulated by ACM2 is lower than YSU in both 15 and 3 km domains (Fig. 3) and the resulting lower precipitation occurs in both domains. The root cause of lower surface temperatures from ACM2 in the nested 3 km domain is

less clear due to the possible effect of 15 km simulations (such as advection) through its lateral boundaries. Thus, the main discussions below (in section b) will focus on further investigation of PBL-clouds-precipitation relationship in the outer 15 km domain with additional simulations with altered treatments, while their relationship at the convection-permitting resolution will be examined with additional single-domain simulations with a 3 km grid spacing (in section c).

b) Impact of different turbulence treatments on clouds and precipitation

Lower troposphere turbulence plays important roles in cloud production and maintenance (Lilly, 1968). This section discusses results of sensitivity simulations adjusting turbulence treatments in YSU and ACM2. Since under clear conditions, ACM2 has stronger daytime boundary layer mixing than YSU (Hu et al., 2010a; Shin & Hong, 2011), vertical mixing in the YSU PBL scheme is first enhanced to see if the simulated clouds and precipitation would become closer to those simulated by ACM2. The exponent p in the K-profile in YSU (default value is 2) is reduced to 0.5 in experiment YSUp.5 to enhance daytime boundary layer mixing, as indicated by the K_z profiles in Fig. 9d. With p=0.5, YSUp.5 simulates higher PBL top height (Fig. 9d). As a result, more near-surface moisture is transported to the top of the elevated PBL, where a thicker cloud layer near the PBL top forms (Fig. 6c & Fig. 9c). Note that while the nonlocal mixing is proportional to K_z in YSU, transilient nonlocal fluxes are explicitly simulated by ACM2, which is not shown in Fig. 9. Thus K_z profiles in Fig. 9d are more indicative of total mixing in the boundary layer for YSU, but less so for ACM2. In the free troposphere where there are no nonlocal mixing treatments for either scheme, thus K_z profiles are indicative of free-troposphere mixing for both.

As the PBL grows in the daytime, the PBL top clouds simulated by both YSU and ACM2 keep elevating (Fig. 5). A more prominent/distinct PBL top cloud layer is simulated by YSU (Fig. 5c,e, PBL top is marked by black dash lines) while the PBL top clouds simulated by ACM2 are indistinctive from the free-troposphere clouds (Fig. 5d,f). Existence of a PBL top cloud layer over the Amazon was previously illustrated by cloud frequency data observed during the GoAmazon 2014/5 field experiments (Giangrande et al., 2017; Giangrande et al., 2020). However, that dataset only provides cloud frequency, not cloud amount. To quantitatively verify the simulated PBL top cloud layer, more advanced cloud dataset is needed.

The thickened PBL top clouds simulated by YSU with p=0.5 weakens surface shortwave radiation (Fig. 7) and consequently lowers surface temperature and CAPE (Fig. 8), thus reduces

precipitation (Fig. 10). Such a precipitation sensitivity to boundary layer mixing over the Amazon is consistent with that reported over the eastern United States (Hu et al., 2018). However, YSU with p=0.5 does not reduce precipitation to the level simulated by ACM2 (Fig. 10). In comparison, ACM2 simulates a more prominent cloud layer at a higher elevation (~4-5 km above ground) while the clouds simulated by YSU at this altitude (with both default p value and p=0.5) weaken in time during the day (Fig. 5). Thus, boundary layer mixing alone cannot completely explain the different impacts of ACM2 and YSU on clouds.

In addition to the different treatments within the boundary layer, ACM2 and YSU also differ in their treatments in the free troposphere. A YSU sensitivity simulation using ACM2's free-troposphere mixing treatment (named YSUuseACM2free) is conducted to examine the impact of free troposphere mixing. YSUuseACM2free simulates a stronger vertical mixing up to 7-8 km above the ground, particularly in presence of clouds, similar to the ACM2 simulation (Fig. 9d). Further up, the sensitivity of vertical mixing is small and K_z is simulated to be less than 0.1 $m^2 s^{-1}$ by all schemes. Thus, our analysis focuses on the lower free troposphere. As a result of stronger mixing in the lower free troposphere, a thicker cloud deck at 4-5 km above ground (Fig. 6d), similar to ACM2 (Fig. 6b), develops in the simulation, likely due to stronger moisture supply from the PBL top. Consequently, surface temperature is reduced due to cloud shield, and the precipitation is reduced, to be closer to that of ACM2 than YSUp. 5 (Fig. 10). Combining both p=0.5 and ACM2's free-troposphere mixing, YSUp. 5useACM2free simulates a similar, but slightly thicker cloud deck (Fig. 6e) and slightly weaker precipitation than YSUuseACM2free (Fig. 10). These experiments illustrate that free-troposphere mixing is the most critical difference between YSU and ACM2 in terms of simulating clouds and precipitation, while the mixing in the PBL plays a secondary role.

For free troposphere vertical mixing, ACM2 and YSU differ in their parameters, moist-air Ri calculation, and the stability functions. Previous studies identified λ as a critical parameter for free-troposphere mixing (Cuxart et al., 2006; Hu et al., 2012; Nielsen-Gammon et al., 2010), and here its impact is further examined. An ACM2 sensitivity simulation with λ=30 (named ACM2λ30) is conducted to verify its impact on clouds/precipitation. Comparing to default ACM2 with λ=80, ACM2λ30 simulates a much weaker mixing in the free troposphere (Fig. 9d), and consequently a much thinner cloud deck at 4-5 km above ground and meanwhile the PBL top clouds appear thicker (Fig. 6f), likely due to weaker vertical transport of moisture from the PBL

top to higher levels. The net result is that the surface radiation is enhanced (Fig. 7f), temperature is higher, and more precipitation is produced (Fig. 10f). The precipitation simulated by ACM2λ30 is not as strong as that simulated by YSU because of other differences in free-troposphere and PBL mixing treatments.

All the above results together suggest a prominent *PBL-free-troposphere moisture relay transport process*: Step 1, boundary layer mixing transports moisture to the PBL top where clouds form; step 2, free-troposphere mixing transports the moisture further to higher levels (~ 4-5 km) to sustain a thick cloud deck at that altitude and reduce the boundary layer top clouds somewhat. *ACM2 simulates a strong PBL-free-troposphere moisture relay transport process.* Comparing to YSU, ACM2 simulates less PBL moisture (by 0.5 g kg^{-1}) and more free troposphere moisture (by 0.2 g kg^{-1} at 3-6.5 km above ground, Fig. 9b) in monthly average. Consequently, the free-troposphere cloud layer is better maintained during daytime. In contrast, the moisture relay transport process simulated by YSU is weaker and the clouds at ~ 4-5 km dissipate quicker during daytime, leading to less cloud coverage, more CAPE and precipitation. Modified YSU with enhanced PBL and free-troposphere mixing (YSUp.5useACM2free) produces similar moisture transport as ACM2 (Fig. 9b,d) hence reduced precipitation. These results suggest that free-troposphere mixing may become prominent in the presence of clouds (which otherwise would be weak as generally regarded) and become an important step in the relay transport process. To verify the strength of such relay transport process, more advanced observations, such as long-term vertical profiles of cloud mixing ratios, are warranted. Our results also suggest that to correctly simulate clouds/precipitation in environments similar to those of the Amazon, the ability of models in reproducing such moisture relay transport processes needs to be carefully assessed.

c) Sensitivity of clouds and precipitation to different turbulence treatments at a convection-allowing resolution

The sensitivity of simulated clouds and precipitation to boundary layer and free-atmosphere vertical mixing discussed above is mainly based on simulations at 15 km grid spacing where cumulus parameterization is employed. Thus, the conclusions are directly applicable to global and regional weather and climate simulations/predictions at convection-parameterized resolutions. Whether these conclusions are still valid at convection-permitting resolutions requires additional examination. To avoid the possible effects of the driving 15 km grid on the nested 3

418 km grid, single-domain sensitivity simulations are conducted that cover a majority of the Amazon
419 with a 3 km grid spacing that use ERA5 data directly as lateral boundary conditions. These
420 simulations include 3kmYSU , 3kmYSUp. 5 , 3kmYSUp. 5useACM2free , and 3kmACM2 (as
421 summarized in Table 1). Even though simulated precipitation rate is generally higher at the 3 km
422 grid spacing than at 15 km grid spacing, the same turbulent mixing → clouds → precipitation
423 impact/sensitivity holds in these convection-permitting simulations (Fig. 11, 12). That is, 1) YSU
424 simulates stronger daytime precipitation rate than ACM2 (by 60% at noon time, 16 vs. 10 mm day-
425 ^{1}, Fig. 12a,b); 2) Stronger boundary layer mixing simulated by YSU with p=0.5 leads to more PBL
426 top clouds (Fig. 11c), which block more shortwave radiation and reduce daytime surface
427 temperature and consequently precipitation (with 13 mm day^{-1} at noon, Fig. 12c); 3) Using the
428 free-troposphere mixing treatment of ACM2 in YSU simulates a more prominent cloud layer at 4-
429 5 km above ground (Fig. 11d) which more effectively blocks shortwave radiation and reduces
430 precipitation (with 11 mm day^{-1} at noon, Fig. 12d) that is closer to the precipitation rate of ACM2
431 (Fig. 12b).
432

433 **4. Conclusions and discussion**

434 Previous studies by others and a recent study of ours found that precipitation simulations
435 over the Amazon in South America are very sensitive to the PBL scheme used. The exact
436 relationship between the turbulent mixing and precipitation processes in that humid region is,
437 however, not clear. In this study, two-month-long simulations over South America in January-
438 February 2019 are examined to understand the precipitation sensitivity to treatments of turbulent
439 mixing in both the PBL and free troposphere within PBL schemes. Two PBL schemes, the YSU
440 and ACM2 schemes, are the foci of this study since they produced the most and least amount of
441 precipitation among PBL schemes examined. Our results serve to disentangle the turbulence –
442 cloud - precipitation processes over the Amazon and reveal root causes for the sensitivity to PBL
443 schemes, which is a prerequisite for future model improvement. During daytime, while the free-
444 troposphere clouds simulated by YSU dissipate due to solar heating, clouds simulated by ACM2
445 maintains through the day because of enhanced moisture supply due to enhanced *PBL-free-*
446 *troposphere* relay transport process: step 1, enhanced vertical mixing within PBL simulated by
447 ACM2 transports surface moisture to the PBL top where clouds first form, and step 2, enhanced
448 free-troposphere mixing feeds the moisture into the free-troposphere cloud deck. Due to the

thicker cloud deck over the Amazon simulated by ACM2, surface radiative heating is reduced and consequently CAPE is reduced. As a result, precipitation is weaker from ACM2. In contrast, the moisture *PBL-free-troposphere* relay transport process simulated by YSU is weaker and the clouds at ~4-5 km dissipate quicker, and CAPE is therefore larger during daytime, leading to more precipitation. To verify the strength of such relay transport process, more advanced observations are warranted, for example, of long-term vertical profiles of cloud mixing ratios. To correctly simulate clouds and precipitation, model performance of reproducing such a moisture relay transport process needs to be carefully evaluated.

Two key parameters dictating the vertical mixing in the YSU and ACM2 schemes are identified, which are p, an exponent in the polynomial function determining boundary layer vertical mixing and λ, the asymptotic length scale dictating free-troposphere mixing. Sensitivity simulations with altered p, λ, and other treatments within YSU and ACM2 confirm the sensitivity of precipitation to the mixing strength. The free-troposphere mixing in presence of clouds become prominent (which is otherwise weak) because of reduced moist static stability and the difference in free-troposphere mixing appears to explain more of the sensitivity to the YSU and ACM2 PBL schemes. The turbulent mixing and cloud relationship over the Amazon simulated with ACM2 suggests strong positive feedback through which regions of lower troposphere clouds create conditions favorable for daytime cloud maintenance. Such feedback is weaker with YSU, which leads to daytime breakup of free-troposphere clouds.

The above results regarding the turbulence-clouds-precipitation processes and their parameterizations have important implications to the understanding and accurate prediction of weather, climate, as well as air quality over the Amazon region that is humid, cloudy and rich in precipitation. South America is experiencing an increasing trend in summer precipitation, and such a trend is also projected by climate models (Vera et al., 2006). Given the negative cloud-precipitation correlation seen in this study for the Amazon region, such a precipitation trend may imply a decreasing trend of cloud cover in the region. Correct representation of turbulence mixing-cloud-radiation interactions within weather and climate models is clearly critical for accurate simulation/prediction of precipitation and water cycles.

Though not shown here, since simulated precipitation is weaker with ACM2, the corresponding tropospheric upward motion is also weaker , so stronger easterly winds impinge on the east side of Andes and are diverted southward to form a stronger southward LLJ east of Andes.

Thus, the simulated strength of Amazonian precipitation is closely linked to the strength of LLJ east of Andes, which may have implications for the simulation of downstream atmospheric environments including temperature and humidity conditions and air quality (Hu et al., 2013b; Hu et al., 2013c; Klein et al., 2014). These are topics for future studies.

Acknowledgments. This work was primarily supported by grant no. 20163646499 from the Universidad Nacional de San Agustín de Arequipa (UNSA) of Peru through the IREES/LASI Global Change and Human Health Institute. The first author is partially supported by the National Mesonet Program grant #10558200 and DOE ASR project (DE-SC0021159). Ming Xue was also supported by NSF grants AGS-1917701. We are grateful to Lan Gao and Jonathan E. Pleim for discussion. The WRF simulations were performed on supercomputers Stampede 2 at the Texas Advanced Computing Center (TACC) through allocations TG-MCA95C006, and TG-ATM160014 from the Advanced Cyberinfrastructure Coordination Ecosystem: Services & Support (ACCESS) program, which is supported by National Science Foundation grants #2138259, #2138286, #2138307, #2137603, and #2138296. The authors also acknowledge high-performance computing support from Cheyenne (https://doi.org/10.5065/D6RX99HX) provided by NCAR's Computational and Information Systems Laboratory. NCAR is sponsored by the National Science Foundation. Some of the post-processing of simulations for this work was performed at the University of Oklahoma (OU) Supercomputing Center for Education and Research (OSCER).

Data Availability Statement.

The ERA5 reanalysis data are available at https://doi.org/10.5065/BH6N-5N20. GPM IMERG Final Precipitation dataset is available at https://doi.org/10.5067/GPM/IMERGDF/DAY/06 (last access: 12 November 2020). CMORPH dataset is available at https://ftp.cpc.ncep.noaa.gov/precip/CMORPH_V1.0/CRT/8km-30min (last access: 12 November 2020). Figures in this manuscript are produced using the NCAR Command Language (Version 6.6.2) [Software]. (2019). Boulder, Colorado: UCAR/NCAR/CISL/TDD. http://dx.doi.org/10.5065/D6WD3XH5 . Model data produced from this study have been archived at CAPS website https://caps.ou.edu/micronet/Regionalclimate.html

References

Adebiyi, A. A., Zuidema, P., Chang, I., Burton, S. P., & Cairns, B. (2020). Mid-level clouds are frequent above the southeast Atlantic stratocumulus clouds. *Atmos. Chem. Phys., 20*(18), 11025-11043. 10.5194/acp-20-11025-2020

Angevine, W. M., Eddington, L., Durkee, K., Fairall, C., Bianco, L., & Brioude, J. (2012). Meteorological Model Evaluation for CalNex 2010. *Monthly Weather Review, 140*(12), 3885-3906. 10.1175/Mwr-D-12-00042.1

Angevine, W. M., Jiang, H. L., & Mauritsen, T. (2010). Performance of an Eddy Diffusivity-Mass Flux Scheme for Shallow Cumulus Boundary Layers. *Monthly Weather Review, 138*(7), 2895-2912. 10.1175/2010mwr3142.1

Barber, K. A., Burleyson, C. D., Feng, Z., & Hagos, S. M. (2022). The Influence of Shallow Cloud Populations on Transitions to Deep Convection in the Amazon. *Journal of the Atmospheric Sciences, 79*(3), 723-743. 10.1175/jas-d-21-0141.1

Beare, R. J., MacVean, M. K., Holtslag, A. A. M., Cuxart, J., Esau, I., Golaz, J. C., . . . Sullivan, P. (2006). An intercomparison of large-eddy simulations of the stable boundary layer. *Boundary-Layer Meteorology, 118*(2), 247-272. 10.1007/s10546-004-2820-6

Bright, D. R., & Mullen, S. L. (2002). The sensitivity of the numerical simulation of the southwest monsoon boundary layer to the choice of PBL turbulence parameterization in MM5. *Weather and Forecasting, 17*(1), 99-114. Doi 10.1175/1520-0434(2002)017<0099:Tsotns>2.0.Co;2

Burleyson, C. D., & Yuter, S. E. (2015). Patterns of Diurnal Marine Stratocumulus Cloud Fraction Variability. *Journal of Applied Meteorology and Climatology, 54*(4), 847-866. 10.1175/jamc-d-14-0178.1

Chakraborty, S., Jiang, J. H., Su, H., & Fu, R. (2020). Deep Convective Evolution From Shallow Clouds Over the Amazon and Congo Rainforests. *Journal of Geophysical Research: Atmospheres, 125*(1), e2019JD030962. https://doi.org/10.1029/2019JD030962

Chakraborty, S., Schiro, K. A., Fu, R., & Neelin, J. D. (2018). On the role of aerosols, humidity, and vertical wind shear in the transition of shallow-to-deep convection at the Green Ocean Amazon 2014/5 site. *Atmos. Chem. Phys., 18*(15), 11135-11148. 10.5194/acp-18-11135-2018

Chen, F., & Zhang, Y. (2009). On the coupling strength between the land surface and the atmosphere: From viewpoint of surface exchange coefficients. *Geophysical Research Letters, 36*. L10404, 10.1029/2009gl037980

Chen, M., Huang, Y., Li, Z., Larico, A. J. M., Xue, M., Hong, Y., . . . Morales, I. Y. (2022). Cross-Examining Precipitation Products by Rain Gauge, Remote Sensing, and WRF Simulations over a South American Region across the Pacific Coast and Andes. *Atmosphere, 13*(10), 1666.

Clark, A. J., Coniglio, M. C., Coffer, B. E., Thompson, G., Xue, M., & Kong, F. Y. (2015). Sensitivity of 24-h Forecast Dryline Position and Structure to Boundary Layer Parameterizations in Convection-Allowing WRF Model Simulations. *Weather and Forecasting, 30*(3), 613-638. 10.1175/Waf-D-14-00078.1

Cohen, A. E., Cavallo, S. M., Coniglio, M. C., & Brooks, H. E. (2015). A Review of Planetary Boundary Layer Parameterization Schemes and Their Sensitivity in Simulating Southeastern US Cold Season Severe Weather Environments. *Weather and Forecasting, 30*(3), 591-612. 10.1175/Waf-D-14-00105.1

555 Coniglio, M. C., Correia, J., Marsh, P. T., & Kong, F. Y. (2013). Verification of Convection-
556 Allowing WRF Model Forecasts of the Planetary Boundary Layer Using Sounding
557 Observations. *Weather and Forecasting, 28*(3), 842-862. 10.1175/Waf-D-12-00103.1
558 Cuxart, J., Holtslag, A. A. M., Beare, R. J., Bazile, E., Beljaars, A., Cheng, A., . . . Xu, K. M.
559 (2006). Single-column model intercomparison for a stably stratified atmospheric
560 boundary layer. *Boundary-Layer Meteorology, 118*(2), 273-303. 10.1007/s10546-005-
561 3780-1
562 Durran, D. R., & Klemp, J. B. (1982). On the Effects of Moisture on the Brunt-Väisälä
563 Frequency. *Journal of Atmospheric Sciences, 39*(10), 2152-2158. 10.1175/1520-
564 0469(1982)039<2152:Oteomo>2.0.Co;2
565 Fu, R., Zhu, B., & Dickinson, R. E. (1999). How Do Atmosphere and Land Surface Influence
566 Seasonal Changes of Convection in the Tropical Amazon? *Journal of Climate, 12*(5),
567 1306-1321. 10.1175/1520-0442(1999)012<1306:Hdaals>2.0.Co;2
568 Giangrande, S. E., Feng, Z., Jensen, M. P., Comstock, J. M., Johnson, K. L., Toto, T., . . . Martin,
569 S. T. (2017). Cloud characteristics, thermodynamic controls and radiative impacts during
570 the Observations and Modeling of the Green Ocean Amazon (GoAmazon2014/5)
571 experiment. *Atmos. Chem. Phys., 17*(23), 14519-14541. 10.5194/acp-17-14519-2017
572 Giangrande, S. E., Wang, D., & Mechem, D. B. (2020). Cloud regimes over the Amazon Basin:
573 perspectives from the GoAmazon2014/5 campaign. *Atmos. Chem. Phys., 20*(12), 7489-
574 7507. 10.5194/acp-20-7489-2020
575 Gunwani, P., & Mohan, M. (2017). Sensitivity of WRF model estimates to various PBL
576 parameterizations in different climatic zones over India. *Atmospheric Research, 194*, 43-
577 65. https://doi.org/10.1016/j.atmosres.2017.04.026
578 Hersbach, H., Bell, B., Berrisford, P., Hirahara, S., Horányi, A., Muñoz-Sabater, J., . . . Thépaut,
579 J.-N. (2020). The ERA5 global reanalysis. *Quarterly Journal of the Royal Meteorological*
580 *Society, 146*(730), 1999-2049. https://doi.org/10.1002/qj.3803
581 Hong, S. Y., Noh, Y., & Dudhia, J. (2006). A new vertical diffusion package with an explicit
582 treatment of entrainment processes. *Monthly Weather Review, 134*(9), 2318-2341. Doi
583 10.1175/Mwr3199.1
584 Hu, X.-M., Doughty, D. C., Sanchez, K. J., Joseph, E., & Fuentes, J. D. (2012). Ozone variability
585 in the atmospheric boundary layer in Maryland and its implications for vertical transport
586 model. *Atmospheric Environment, 46*, 354-364. 10.1016/j.atmosenv.2011.09.054
587 Hu, X.-M., Klein, P. M., & Xue, M. (2013a). Evaluation of the updated YSU planetary boundary
588 layer scheme within WRF for wind resource and air quality assessments. *Journal of*
589 *Geophysical Research-Atmospheres, 118*(18), 10490-10505. 10.1002/jgrd.50823
590 Hu, X.-M., Klein, P. M., Xue, M., Lundquist, J. K., Zhang, F., & Qi, Y. (2013b). Impact of Low-
591 Level Jets on the Nocturnal Urban Heat Island Intensity in Oklahoma City. *Journal of*
592 *Applied Meteorology and Climatology, 52*(8), 1779-1802. 10.1175/jamc-d-12-0256.1
593 Hu, X.-M., Klein, P. M., Xue, M., Zhang, F., Doughty, D. C., Forkel, R., . . . Fuentes, J. D.
594 (2013c). Impact of the vertical mixing induced by low-level jets on boundary layer ozone
595 concentration. *Atmospheric Environment, 70*, 123-130. 10.1016/j.atmosenv.2012.12.046
596 Hu, X.-M., Nielsen-Gammon, J. W., & Zhang, F. Q. (2010a). Evaluation of Three Planetary
597 Boundary Layer Schemes in the WRF Model. *Journal of Applied Meteorology and*
598 *Climatology, 49*(9), 1831-1844. 10.1175/2010jamc2432.1
599 Hu, X.-M., Xue, M., & Li, X. (2019). The Use of High-Resolution Sounding Data to Evaluate
600 and Optimize Nonlocal PBL Schemes for Simulating the Slightly Stable Upper

Convective Boundary Layer. *Monthly Weather Review, 147*(10), 3825-3841. 10.1175/mwr-d-19-0085.1

Hu, X.-M., Xue, M., McPherson, R. A., Martin, E., Rosendahl, D. H., & Qiao, L. (2018). Precipitation Dynamical Downscaling Over the Great Plains. *Journal of Advances in Modeling Earth Systems, 10*(2), 421-447. 10.1002/2017ms001154

Hu, X.-M., Zhang, F., & Nielsen-Gammon, J. W. (2010b). Ensemble-based simultaneous state and parameter estimation for treatment of mesoscale model error: A real-data study. *Geophysical Research Letters, 37*. L08802, 10.1029/2010gl043017

Huang, H. Y., Hall, A., & Teixeira, J. (2013). Evaluation of the WRF PBL Parameterizations for Marine Boundary Layer Clouds: Cumulus and Stratocumulus. *Monthly Weather Review, 141*(7), 2265-2271. 10.1175/Mwr-D-12-00292.1

Huang, Y., Xue, M., Hu, X.-M., Martin, E. R., Novoa, H., McPherson, R. A., . . . Morales, I. Y. (2022). *Characteristics of Precipitation and MCS over the Peruvian Central Andes based on Convection-Permitting Simulations.* Paper presented at the AGU fall meeting, Chicago, IL, https://agu.confex.com/agu/fm22/meetingapp.cgi/Person/177979.

Huffman, G. J., E.F. Stocker, D.T. Bolvin, Nelkin, E. J., & Tan, J. (2019). GPM IMERG Final Precipitation L3 1 day 0.1 degree x 0.1 degree V06 (Publication no. https://doi.org/10.5067/GPM/IMERGDF/DAY/06). Retrieved Nov. 2022

Iacono, M. J., Delamere, J. S., Mlawer, E. J., Shephard, M. W., Clough, S. A., & Collins, W. D. (2008). Radiative forcing by long-lived greenhouse gases: Calculations with the AER radiative transfer models. *Journal of Geophysical Research: Atmospheres, 113*(D13). https://doi.org/10.1029/2008JD009944

Jankov, I., Gallus, W. A., Segal, M., Shaw, B., & Koch, S. E. (2005). The impact of different WRF model physical parameterizations and their interactions on warm season MCS rainfall. *Weather and Forecasting, 20*(6), 1048-1060. Doi 10.1175/Waf888.1

Jankov, I., Schultz, P. J., Anderson, C. J., & Koch, S. E. (2007). The Impact of Different Physical Parameterizations and Their Interactions on Cold Season QPF in the American River Basin. *Journal of Hydrometeorology, 8*(5), 1141-1151. 10.1175/jhm630.1

Jiménez, P. A., Dudhia, J., González-Rouco, J. F., Navarro, J., Montávez, J. P., & García-Bustamante, E. (2012). A Revised Scheme for the WRF Surface Layer Formulation. *Monthly Weather Review, 140*(3), 898-918. 10.1175/mwr-d-11-00056.1

Joyce, R. J., Janowiak, J. E., Arkin, P. A., & Xie, P. (2004). CMORPH: A Method that Produces Global Precipitation Estimates from Passive Microwave and Infrared Data at High Spatial and Temporal Resolution. *Journal of Hydrometeorology, 5*(3), 487-503. 10.1175/1525-7541(2004)005<0487:Camtpg>2.0.Co;2

Kay, J. E., Bourdages, L., Miller, N. B., Morrison, A., Yettella, V., Chepfer, H., & Eaton, B. (2016). Evaluating and improving cloud phase in the Community Atmosphere Model version 5 using spaceborne lidar observations. *Journal of Geophysical Research: Atmospheres, 121*(8), 4162-4176. https://doi.org/10.1002/2015JD024699

Kay, J. E., Hillman, B. R., Klein, S. A., Zhang, Y., Medeiros, B., Pincus, R., . . . Ackerman, T. P. (2012). Exposing Global Cloud Biases in the Community Atmosphere Model (CAM) Using Satellite Observations and Their Corresponding Instrument Simulators. *Journal of Climate, 25*(15), 5190-5207. 10.1175/jcli-d-11-00469.1

Klein, P. M., Hu, X. M., & Xue, M. (2014). Impacts of Mixing Processes in Nocturnal Atmospheric Boundary Layer on Urban Ozone Concentrations. *Boundary-Layer Meteorology, 150*(1), 107-130. 10.1007/s10546-013-9864-4

Langenbrunner, B., Pritchard, M. S., Kooperman, G. J., & Randerson, J. T. (2019). Why Does Amazon Precipitation Decrease When Tropical Forests Respond to Increasing CO2? *Earth's Future, 7*(4), 450-468. https://doi.org/10.1029/2018EF001026

Li, X. L., & Pu, Z. X. (2008). Sensitivity of Numerical Simulation of Early Rapid Intensification of Hurricane Emily (2005) to Cloud Microphysical and Planetary Boundary Layer Parameterizations. *Monthly Weather Review, 136*(12), 4819-4838. 10.1175/2008mwr2366.1

Lilly, D. K. (1968). Models of Cloud-Topped Mixed Layers under a Strong Inversion. *Quarterly Journal of the Royal Meteorological Society, 94*(401), 292-&. DOI 10.1002/qj.49709440106

Liu, C., Ikeda, K., Rasmussen, R., Dominguez, F., Prein, A. F., Dudhia, J., & Chen, F. (2022). *An Overview of Two-Decade-Long Convection Permitting Regional Climate Downscaling over the Continental South America.* Paper presented at the AGU fall meeting, Chicago, IL, https://agu.confex.com/agu/fm22/meetingapp.cgi/Paper/1115319.

Liu, M., & Carroll, J. J. (1996). A high-resolution air pollution model suitable for dispersion studies in complex terrain. *Monthly Weather Review, 124*(10), 2396-2409. Doi 10.1175/1520-0493(1996)124<2396:Ahrapm>2.0.Co;2

Lu, X., & Wang, X. (2019). Improving Hurricane Analyses and Predictions with TCI, IFEX Field Campaign Observations, and CIMSS AMVs Using the Advanced Hybrid Data Assimilation System for HWRF. Part I: What is Missing to Capture the Rapid Intensification of Hurricane Patricia (2015) when HWRF is already Initialized with a More Realistic Analysis? *Monthly Weather Review, 147*(4), 1351-1373. 10.1175/mwr-d-18-0202.1

Miguez-Macho, G., Stenchikov, G. L., & Robock, A. (2004). Spectral nudging to eliminate the effects of domain position and geometry in regional climate model simulations. *Journal of Geophysical Research-Atmospheres, 109*(D13). D13104, 10.1029/2003jd004495

Miguez-Macho, G., Stenchikov, G. L., & Robock, A. (2005). Regional climate simulations over North America: Interaction of local processes with improved large-scale flow. *Journal of Climate, 18*(8), 1227-1246. Doi 10.1175/Jcli3369.1

Nakanishi, M., & Niino, H. (2006). An Improved Mellor–Yamada Level-3 Model: Its Numerical Stability and Application to a Regional Prediction of Advection Fog. *Boundary-Layer Meteorology, 119*(2), 397-407. 10.1007/s10546-005-9030-8

Nielsen-Gammon, J. W., Hu, X.-M., Zhang, F., & Pleim, J. E. (2010). Evaluation of Planetary Boundary Layer Scheme Sensitivities for the Purpose of Parameter Estimation. *Monthly Weather Review, 138*(9), 3400-3417. 10.1175/2010mwr3292.1

Noh, Y., Cheon, W. G., Hong, S. Y., & Raasch, S. (2003). Improvement of the K-profile model for the planetary boundary layer based on large eddy simulation data. *Boundary-Layer Meteorology, 107*(2), 401-427. Doi 10.1023/A:1022146015946

Olson, J. B., Kenyon, J. S., Angevine, W. A., Brown, J. M., Pagowski, M., & Sušelj, K. (2019a). A Description of the MYNN-EDMF Scheme and the Coupling to Other Components in WRF–ARW. https://doi.org/10.25923/n9wm-be49

Olson, J. B., Kenyon, J. S., Djalalova, I., Bianco, L., Turner, D. D., Pichugina, Y., . . . Cline, J. (2019b). Improving Wind Energy Forecasting through Numerical Weather Prediction Model Development. *Bulletin of the American Meteorological Society, 100*(11), 2201-2220. 10.1175/bams-d-18-0040.1

692 Painemal, D., Xu, K.-M., Cheng, A., Minnis, P., & Palikonda, R. (2015). Mean Structure and
693 Diurnal Cycle of Southeast Atlantic Boundary Layer Clouds: Insights from Satellite
694 Observations and Multiscale Modeling Framework Simulations. *Journal of Climate,*
695 *28*(1), 324-341. 10.1175/jcli-d-14-00368.1
696 Pergaud, J., Masson, V., Malardel, S., & Couvreux, F. (2009). A parameterization of dry
697 thermals and shallow cumuli for mesoscale numerical weather prediction. *Bound.-Layer*
698 *Meteor., 132*, 83-106.
699 Pleim, J. E. (2007). A combined local and nonlocal closure model for the atmospheric boundary
700 layer. Part I: Model description and testing. *Journal of Applied Meteorology and*
701 *Climatology, 46*(9), 1383-1395. 10.1175/Jam2539.1
702 Prein, A. F., Ge, M., Valle, A. R., Wang, D., & Giangrande, S. E. (2022). Towards a Unified
703 Setup to Simulate Mid-Latitude and Tropical Mesoscale Convective Systems at
704 Kilometer-Scales. *Earth and Space Science, 9*(8), e2022EA002295.
705 https://doi.org/10.1029/2022EA002295
706 Prein, A. F., Langhans, W., Fosser, G., Ferrone, A., Ban, N., Goergen, K., . . . Leung, R. (2015).
707 A review on regional convection-permitting climate modeling: Demonstrations,
708 prospects, and challenges. *Reviews of Geophysics, 53*(2), 323-361.
709 Prein, A. F., Rasmussen, R. M., Ikeda, K., Liu, C., Clark, M. P., & Holland, G. J. (2017). The
710 future intensification of hourly precipitation extremes. *Nature Clim. Change, 7*(1), 48-52.
711 10.1038/nclimate3168,
712 http://www.nature.com/nclimate/journal/v7/n1/abs/nclimate3168.html#supplementary-
713 information
714 Shin, H. H., & Hong, S. Y. (2011). Intercomparison of Planetary Boundary-Layer
715 Parametrizations in the WRF Model for a Single Day from CASES-99. *Boundary-Layer*
716 *Meteorology, 139*(2), 261-281. 10.1007/s10546-010-9583-z
717 Skamarock, W. C., & Klemp, J. B. (2008). A time-split nonhydrostatic atmospheric model for
718 weather research and forecasting applications. *Journal of Computational Physics, 227*(7),
719 3465-3485. http://dx.doi.org/10.1016/j.jcp.2007.01.037
720 Skamarock, W. C., Klemp, J. B., Dudhia, J., Gill, D. O., Liu, Z., Berner, J., . . . Huang, X.-y.
721 (2021). *A Description of the Advanced Research WRF Model Version 4.3*. (NCAR/TN-
722 556+STR). Retrieved from http://dx.doi.org/10.5065/1dfh-6p97.
723 Sun, X. G., Xue, M., Brotzge, J., McPherson, R. A., Hu, X. M., & Yang, X. Q. (2016). An
724 evaluation of dynamical downscaling of Central Plains summer precipitation using a
725 WRF-based regional climate model at a convection-permitting 4km resolution. *Journal of*
726 *Geophysical Research-Atmospheres, 121*(23), 13801-13825. 10.1002/2016jd024796
727 Supinie, T. A., Park, J., Snook, N., Hu, X. M., Brewster, K. A., Xue, M., & Carley, J. R. (2022).
728 Cool-Season Evaluation of FV3-LAM-Based CONUS-Scale Forecasts with Physics
729 Configurations of Experimental RRFS Ensembles. *Monthly Weather Review, 150*(9),
730 2379-2398. 10.1175/mwr-d-21-0331.1
731 Tai, S.-L., Feng, Z., Ma, P.-L., Schumacher, C., & Fast, J. D. (2021). Representations of
732 Precipitation Diurnal Cycle in the Amazon as Simulated by Observationally Constrained
733 Cloud-System Resolving and Global Climate Models. *Journal of Advances in Modeling*
734 *Earth Systems, 13*(11), e2021MS002586. https://doi.org/10.1029/2021MS002586
735 Thompson, G., Field, P. R., Rasmussen, R. M., & Hall, W. D. (2008). Explicit Forecasts of
736 Winter Precipitation Using an Improved Bulk Microphysics Scheme. Part II:

737 Implementation of a New Snow Parameterization. *Monthly Weather Review, 136*(12),
738 5095-5115. 10.1175/2008mwr2387.1
739 Tiedtke, M. (1989). A Comprehensive Mass Flux Scheme for Cumulus Parameterization in
740 Large-Scale Models. *Monthly Weather Review, 117*(8), 1779-1800. Doi 10.1175/1520-
741 0493(1989)117<1779:Acmfsf>2.0.Co;2
742 Troen, I., & Mahrt, L. (1986). A Simple-Model of the Atmospheric Boundary-Layer - Sensitivity
743 to Surface Evaporation. *Boundary-Layer Meteorology, 37*(1-2), 129-148. Doi
744 10.1007/Bf00122760
745 Vera, C., Silvestri, G., Liebmann, B., & González, P. (2006). Climate change scenarios for
746 seasonal precipitation in South America from IPCC-AR4 models. *Geophysical Research*
747 *Letters, 33*(13). https://doi.org/10.1029/2006GL025759
748 Wang, J. L., & Kotamarthi, V. R. (2013). Assessment of Dynamical Downscaling in Near-
749 Surface Fields with Different Spectral Nudging Approaches Using the Nested Regional
750 Climate Model (NRCM). *Journal of Applied Meteorology and Climatology, 52*(7), 1576-
751 1591. 10.1175/Jamc-D-12-0302.1
752 Wang, J. X., & Hu, X. M. (2021). Evaluating the Performance of WRF Urban Schemes and PBL
753 Schemes over Dallas-Fort Worth during a Dry Summer and a Wet Summer. *Journal of*
754 *Applied Meteorology and Climatology, 60*(6), 779-798. 10.1175/Jamc-D-19-0195.1
755 Wang, W. G., Shen, X. Y., & Huang, W. Y. (2016). A Comparison of Boundary-Layer
756 Characteristics Simulated Using Different Parametrization Schemes. *Boundary-Layer*
757 *Meteorology, 161*(2), 375-403. 10.1007/s10546-016-0175-4
758 Wright, J. S., Fu, R., Worden, J. R., Chakraborty, S., Clinton, N. E., Risi, C., . . . Yin, L. (2017).
759 Rainforest-initiated wet season onset over the southern Amazon. *Proceedings of the*
760 *National Academy of Sciences, 114*(32), 8481-8486. doi:10.1073/pnas.1621516114
761 Wu, M., Lee, J.-E., Wang, D., & Salameh, M. (2021a). Suppressed Daytime Convection Over
762 the Amazon River. *Journal of Geophysical Research: Atmospheres, 126*(13),
763 e2020JD033627. https://doi.org/10.1029/2020JD033627
764 Wu, Z., Li, Y., Li, X., Hu, X.-M., Zhou, G., & Deng, C. (2021b). Influence of Different
765 Planetary Boundary Layer Parameterization Schemes on the Simulation of Precipitation
766 Caused by Southwest China Vortex in Sichuan Basin Based on the WRF Model. *Chinese*
767 *Journal of Atmospheric Sciences, 45*(1), 58. 10.3878/j.issn.1006-9895.2005.19171
768 Xie, B., Fung, J. C. H., Chan, A., & Lau, A. (2012). Evaluation of nonlocal and local planetary
769 boundary layer schemes in the WRF model. *Journal of Geophysical Research:*
770 *Atmospheres, 117*(D12). https://doi.org/10.1029/2011JD017080
771 Yang, Y., Hu, X.-M., Gao, S., & Wang, Y. (2019). Sensitivity of WRF simulations with the YSU
772 PBL scheme to the lowest model level height for a sea fog event over the Yellow Sea.
773 *Atmospheric Research, 215*, 253-267. https://doi.org/10.1016/j.atmosres.2018.09.004
774 Zhang, D., Wang, Z., & Liu, D. (2010). A global view of midlevel liquid-layer topped stratiform
775 cloud distribution and phase partition from CALIPSO and CloudSat measurements.
776 *Journal of Geophysical Research: Atmospheres, 115*(D4).
777 https://doi.org/10.1029/2009JD012143
778 Zhang, Y., Jiang, Y., & Tan, B. (2013). Influences of different PBL schemes on secondary
779 eyewall formation and eyewall replacement cycle in simulated Typhoon Sinlaku (2008).
780 *Acta Meteorologica Sinica, 27*, 322-334. 10.1007/s13351-013-0312-7
781 Zhu, P., Hazelton, A., Zhang, Z., Marks, F. D., & Tallapragada, V. (2021). The Role of Eyewall
782 Turbulent Transport in the Pathway to Intensification of Tropical Cyclones. *Journal of*

Geophysical Research: Atmospheres, 126(17), e2021JD034983. https://doi.org/10.1029/2021JD034983

Zhu, P., Tyner, B., Zhang, J. A., Aligo, E., Gopalakrishnan, S., Marks, F. D., . . . Tallapragada, V. (2019). Role of eyewall and rainband eddy forcing in tropical cyclone intensification. *Atmos. Chem. Phys., 19*(22), 14289-14310. 10.5194/acp-19-14289-2019

Table 1. Model configuration for sensitivity simulations modifying parameters and treatments in the YSU and ACM2 PBL schemes. p is an exponent in the polynomial function determining vertical mixing strength in the PBL, λ is the asymptotic length scale.

PBL	**Grid spacings**	**Experiment name**	**Changed parameters/treatments**
YSU	15 km	YSU	$p=2$ (default)
		YSUp.5	$p=0.5$
		YSUuseACM2free	Use free troposphere treatment from ACM2
		YSUp.5useACM2free	$p=0.5$ & use free troposphere treatment from ACM2
	3km	3kmYSU	$p=2$ (default)
		3kmYSUp.5	$p=0.5$
		3kmYSUp.5useACM2free	$p=0.5$ & use free troposphere treatment from ACM2
ACM2	15 km	ACM2	$\lambda=80$ (default)
		ACM2λ30	$\lambda=30$
	3 km	3kmACM2	$\lambda=80$ (default)

Figures

Figure 1. Daily mean precipitation rate in Jan-Feb 2019 simulated with (a) YSU in domain 1, (b) ACM2 in domain 1 with a 15 km grid spacing, (c) YSU in domain 2, (d) ACM2 in domain 2 with a 3 km grid spacing, (e) single-domain YSU, (f) single-domain ACM2 with a 3 km grid spacing and from (g) IMERG, (h) CMORPH data. The rectangle in (a) marks the location of the nested domain.

Figure 2. Hourly mean precipitation rate at 18 UTC (14 LST) in Jan-Feb 2019 simulated with (a) YSU in domain 1, (b) ACM2 in domain 1, (c) YSU in domain 2, (d) ACM2 in domain 2, (e) single-domain YSU, (f) single-domain ACM2 and observed from (g) IMERG, (h) CMORPH.

Figure 3. Average surface temperature at 17 UTC in Jan-Feb 2019 from (a,c,e) YSU, (b,d,f) ACM2, and (g,h,i) their difference (ACM2-YSU) in (top to bottom) different domains. The average difference over land is marked at the lower-left corner in (g,h,i)

Figure 4. Average surface downward shortwave radiation at 17 UTC in Jan-Feb 2019 simulated with (a,c,e) YSU, (b,d,f) ACM2, (g,h,i) their difference, and (j,k,l) column-average cloud water mixing ratios in (top to bottom) different domains. The straight dash lines mark the location of cross-sections in Figs. 5, 6, and 11.

Figure 5. Cross-section of cloud water over the Amazon in Jan-Feb 2019 simulated by (left) YSU and (right) ACM2 at (a,b) 11, (c,d) 14, (e,f) 17, and (g,h) 21 UTC (7, 10, 13, 17 LST correspondingly). The location of these cross-sections is marked in Fig. 4j

Figure 6. Cross-section of cloud water over the Amazon in Jan-Feb 2019 simulated by (a) YSU and (b) ACM2, (c) $YSUp.5$, (d) $YSUuseACM2free$, (e) $YSUp.5useACM2free$, (f) ACM2λ30 at 17 UTC. The location of these cross-sections is marked in Fig. 4j

Figure 7. Average surface downward shortwave radiation at 17 UTC during January-February 2019 simulated by (a) YSU, (b) ACM2 and 4 sensitivity simulations (c) $YSUp.5$, (d) $YSUuseACM2free$, (e) $YSUp.5useACM2free$, (f) ACM2λ30.

Figure 8. Average CAPE at 17 UTC during January-February 2019 simulated by (a) YSU, (b) ACM2 and 4 sensitivity simulations (c) $YSUp.5$, (d) $YSUuseACM2free$, (e) $YSUp.5useACM2free$, (f) ACM2λ30.

Figure 9. Mean profiles of (a) water vapor mixing ratio, (b) water vapor difference from that simulated by YSU, (c) cloud water mixing ratio (QCLOUD), and (d) vertical mixing coefficient (K_z) at 17 UTC during January-February 2019 at Manaus (location marked in Fig. 8b) simulated by YSU, ACM2 and 4 sensitivity simulations $YSUp.5$, $YSUuseACM2free$, $YSUp.5useACM2free$, ACM2λ30.

Figure 10. Average precipitation rate at 18 UTC during January-February 2019 simulated by (a) YSU, (b) ACM2 and 4 sensitivity simulations (c) $YSUp.5$, (d) $YSUuseACM2free$, (e) $YSUp.5useACM2free$, (f) ACM2λ30.

Figure 11. Cross-section of average noon-time cloud water mixing ratios over the Amazon in Jan-Feb 2019 simulated by (a) $3kmYSU$, (b) $3kmACM2$, (c) $3kmYSUp.5$, and (d) $3kmYSUp.5useACM2free$. The location of these cross-sections is marked in Fig. 4l

Figure 12. Average noon-time precipitation rate in Jan-Feb 2019 simulated by (a) $3kmYSU$, (b) $3kmACM2$, (c) $3kmYSUp.5$, and (d) $3kmYSUp.5useACM2free$. The domain-averaged values are marked.

Figures.

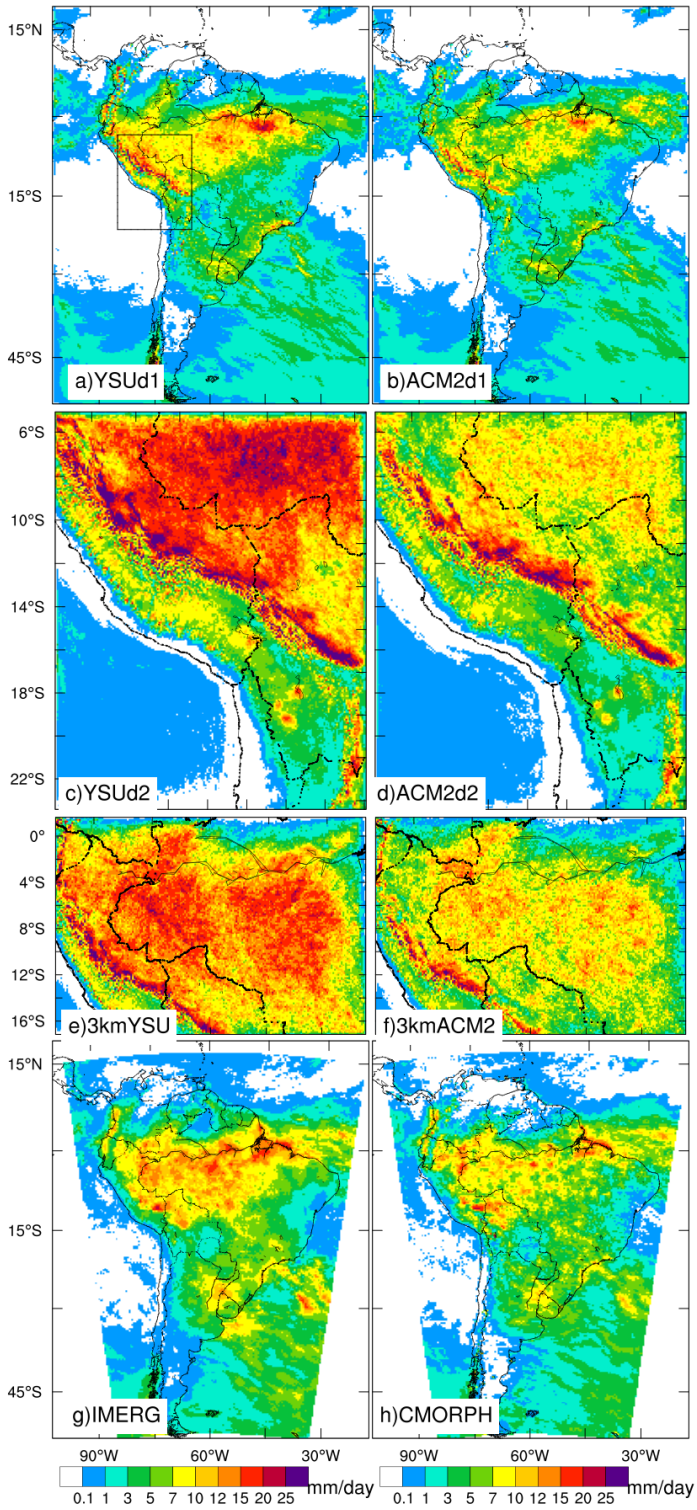

Figure 1. Daily mean precipitation rate in Jan-Feb 2019 simulated with (a) YSU in domain 1, (b) ACM2 in domain 1 with a 15 km grid spacing, (c) YSU in domain 2, (d) ACM2 in domain 2 with a 3 km grid spacing, (e) single-domain YSU, (f) single-domain ACM2 with a 3 km grid spacing and from (g) IMERG, (h) CMORPH data. The rectangle in (a) marks the location of the nested domain.

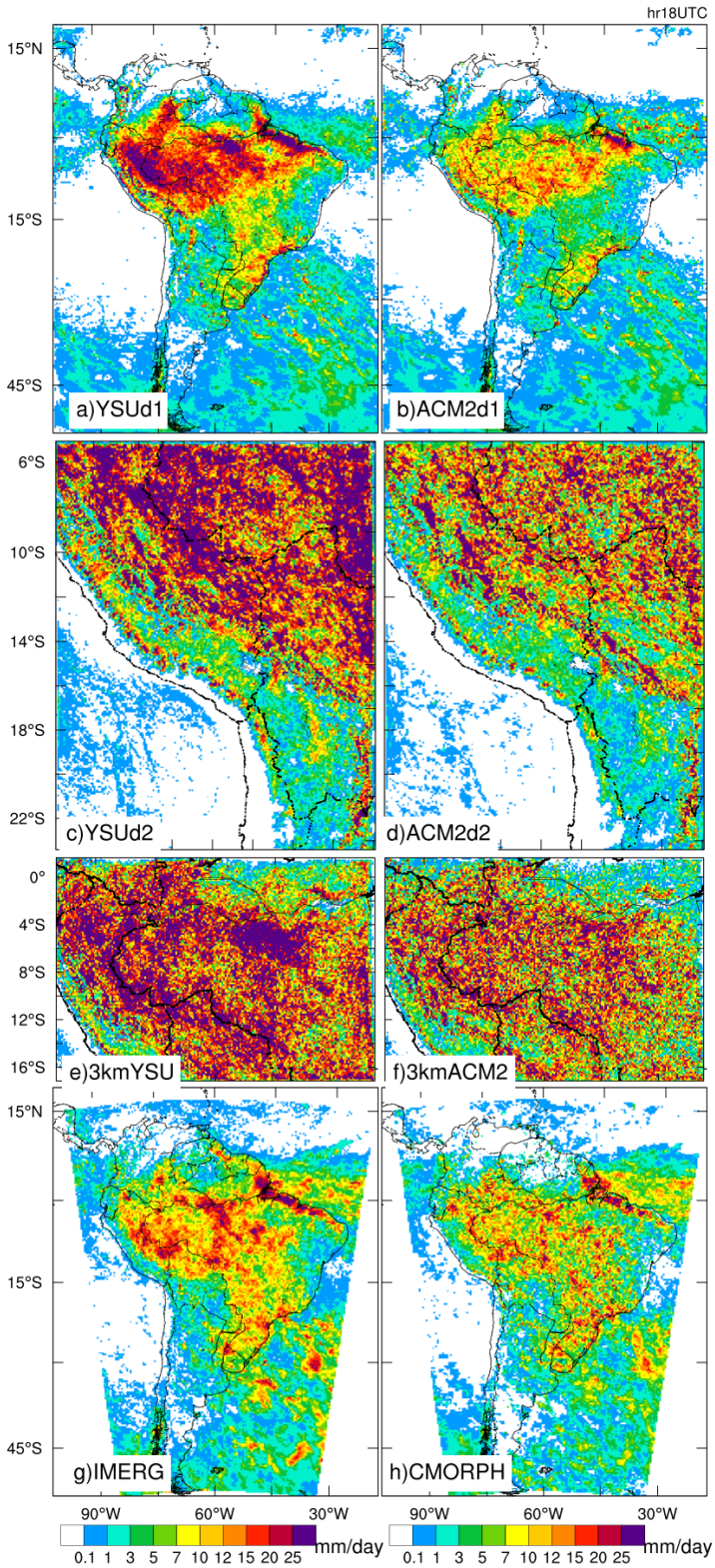

Figure 2. Hourly mean precipitation rate at 18 UTC (14 LST) in Jan-Feb 2019 simulated with (a) YSU in domain 1, (b) ACM2 in domain 1, (c) YSU in domain 2, (d) ACM2 in domain 2, (e) single-domain YSU, (f) single-domain ACM2 and observed from (g) IMERG, (h) CMORPH.

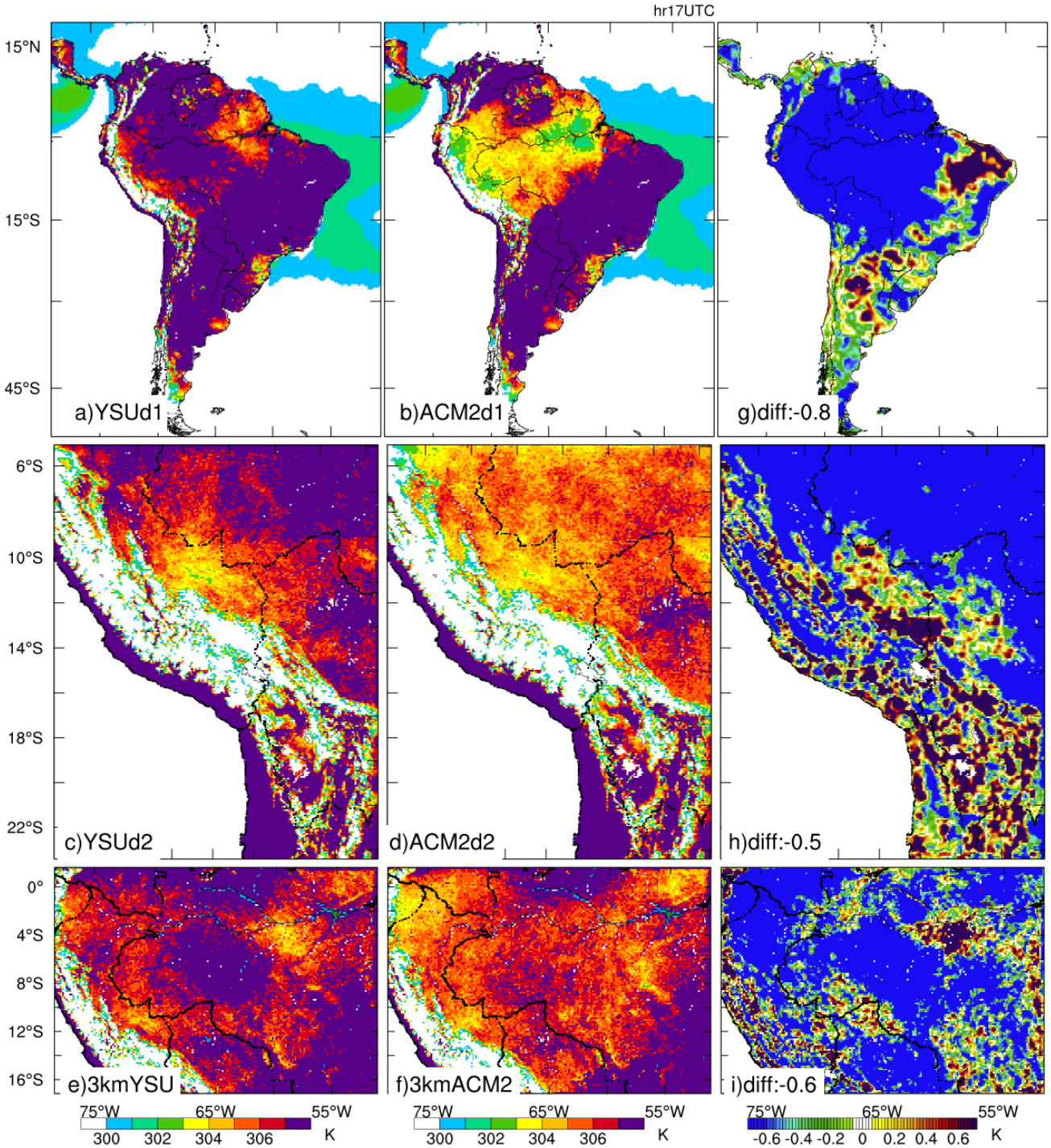

Figure 3. Average surface temperature at 17 UTC in Jan-Feb 2019 from (a,c,e) YSU, (b,d,f) ACM2, and (g,h,i) their difference (ACM2-YSU) in (top to bottom) different domains. The average difference over land is marked at the lower-left corner in (g,h,i)

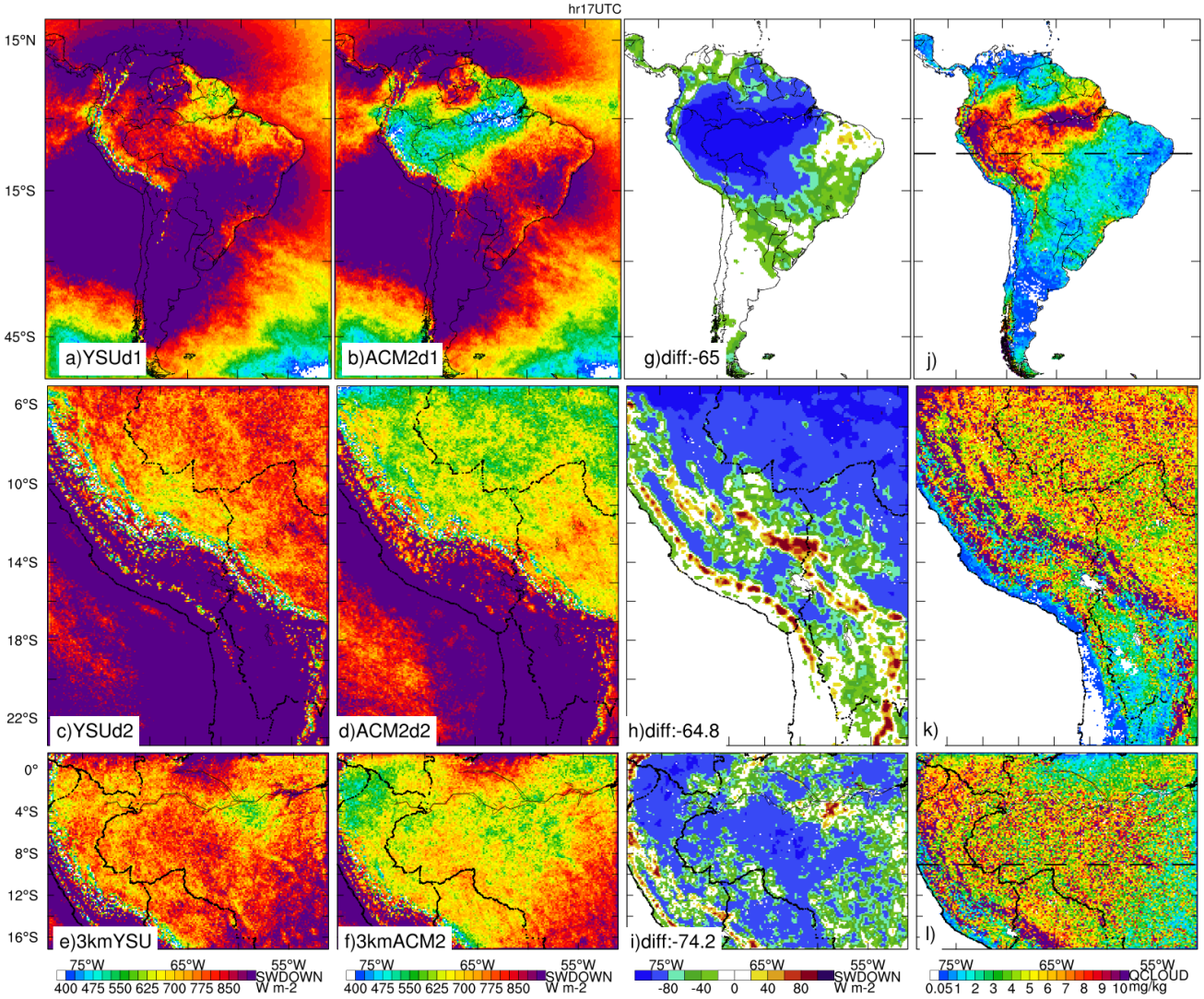

Figure 4. Average surface downward shortwave radiation at 17 UTC in Jan-Feb 2019 simulated with (a,c,e) YSU, (b,d,f) ACM2, (g,h,i) their difference, and (j,k,l) column-average cloud water mixing ratios in (top to bottom) different domains. The straight dash lines mark the location of cross-sections in Figs. 5, 6, and 11.

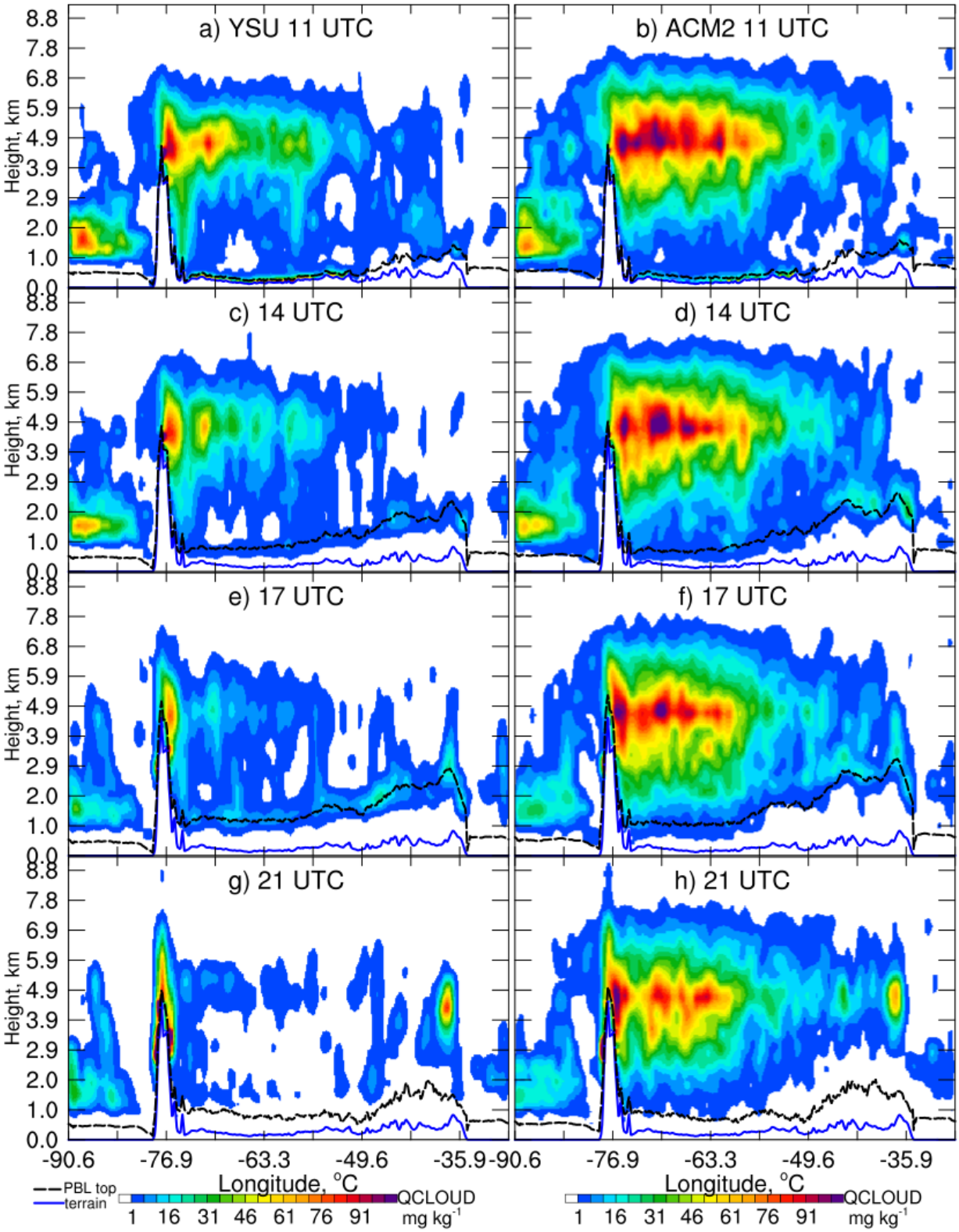

Figure 5. Cross-section of cloud water over the Amazon in Jan-Feb 2019 simulated by (left) YSU and (right) ACM2 at (a,b) 11, (c,d) 14, (e,f) 17, and (g,h) 21 UTC (7, 10, 13, 17 LST correspondingly). The location of these cross-sections is marked in Fig. 4j

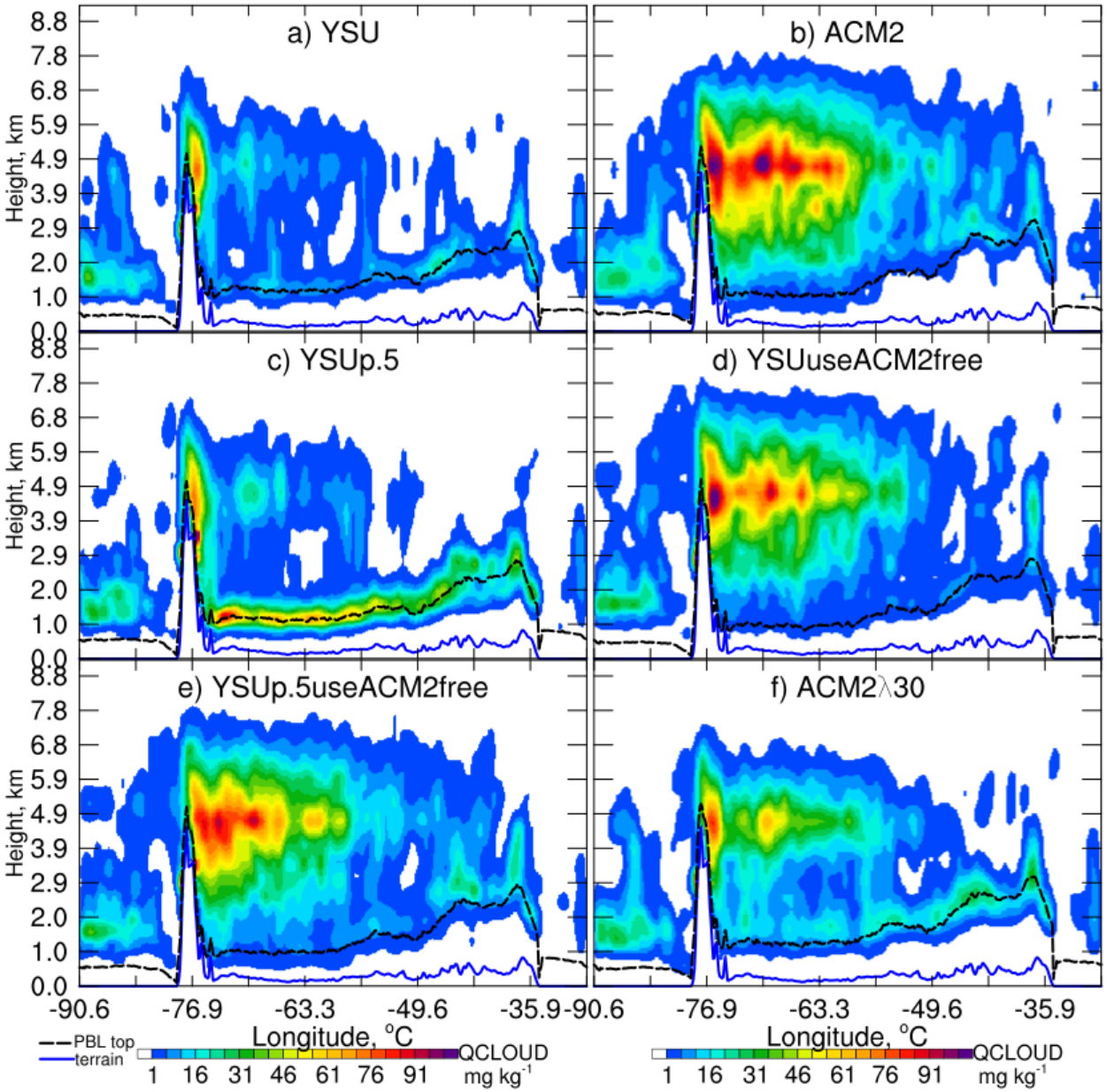

Figure 6. Cross-section of cloud water over the Amazon in Jan-Feb 2019 simulated by (a) YSU and (b) ACM2, (c) YSUp. 5, (d) YSUuseACM2free, (e) YSUp. 5useACM2free, (f) ACM2λ30 at 17 UTC. The location of these cross-sections is marked in Fig. 4j

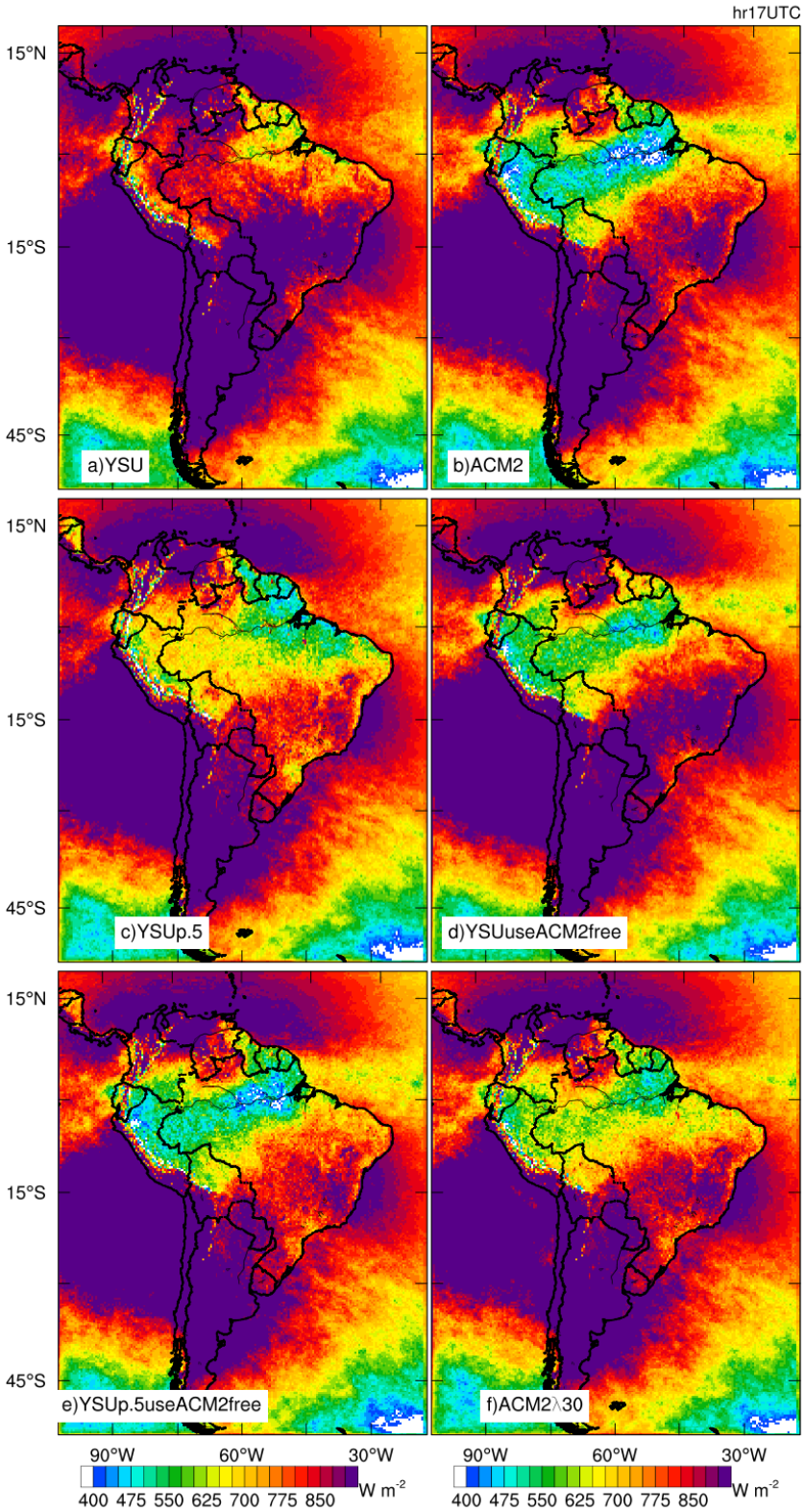

Figure 7. Average surface downward shortwave radiation at 17 UTC during January-February 2019 simulated by (a) YSU, (b) ACM2 and 4 sensitivity simulations (c) YSUp.5, (d) YSUuseACM2free, (e) YSUp.5useACM2free, (f) ACM2λ30.

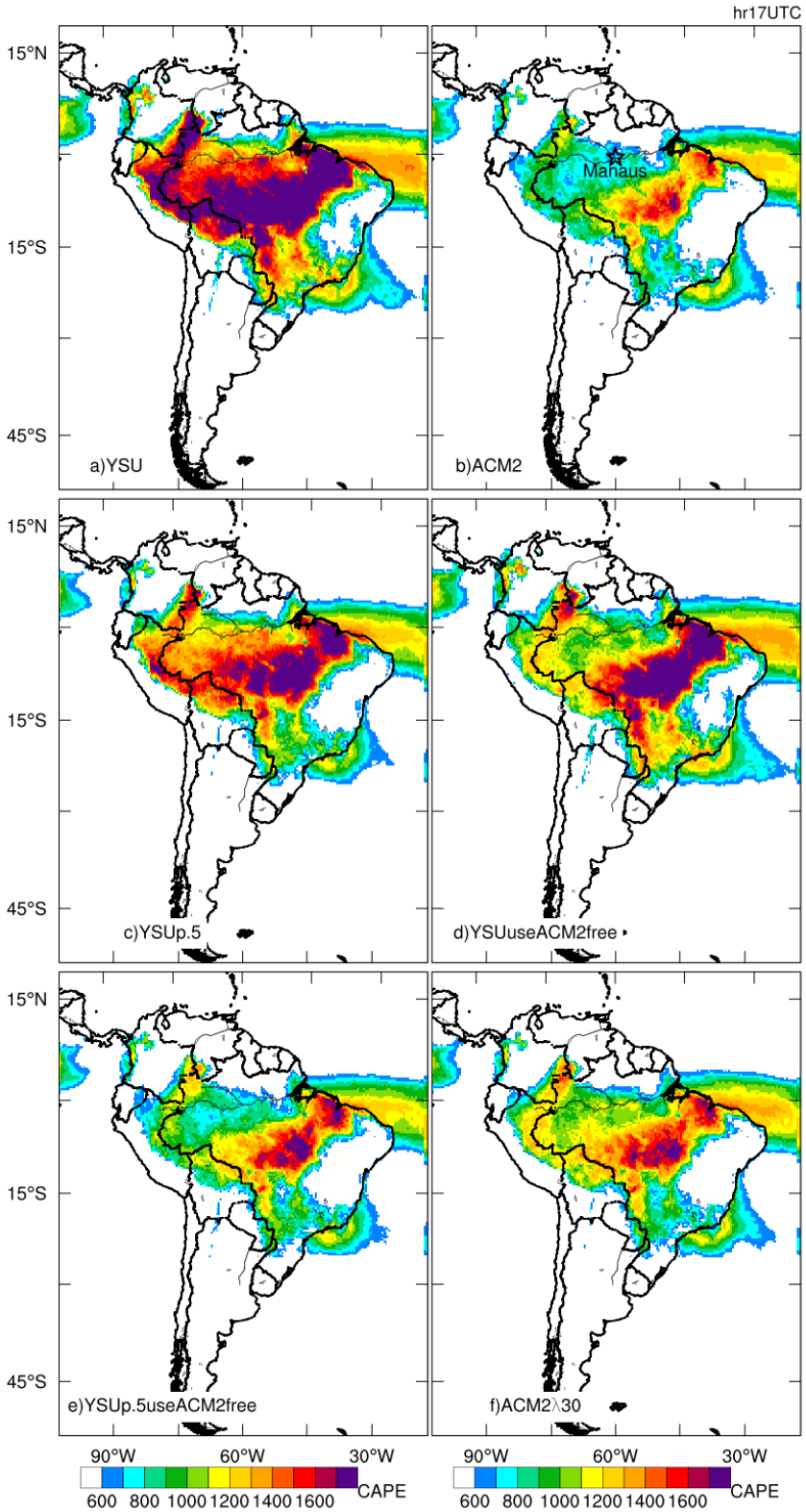

Figure 8. Average CAPE at 17 UTC during January-February 2019 simulated by (a) YSU, (b) ACM2 and 4 sensitivity simulations (c) YSUp. 5, (d) YSUuseACM2free, (e) YSUp. 5useACM2free, (f) ACM2λ30.

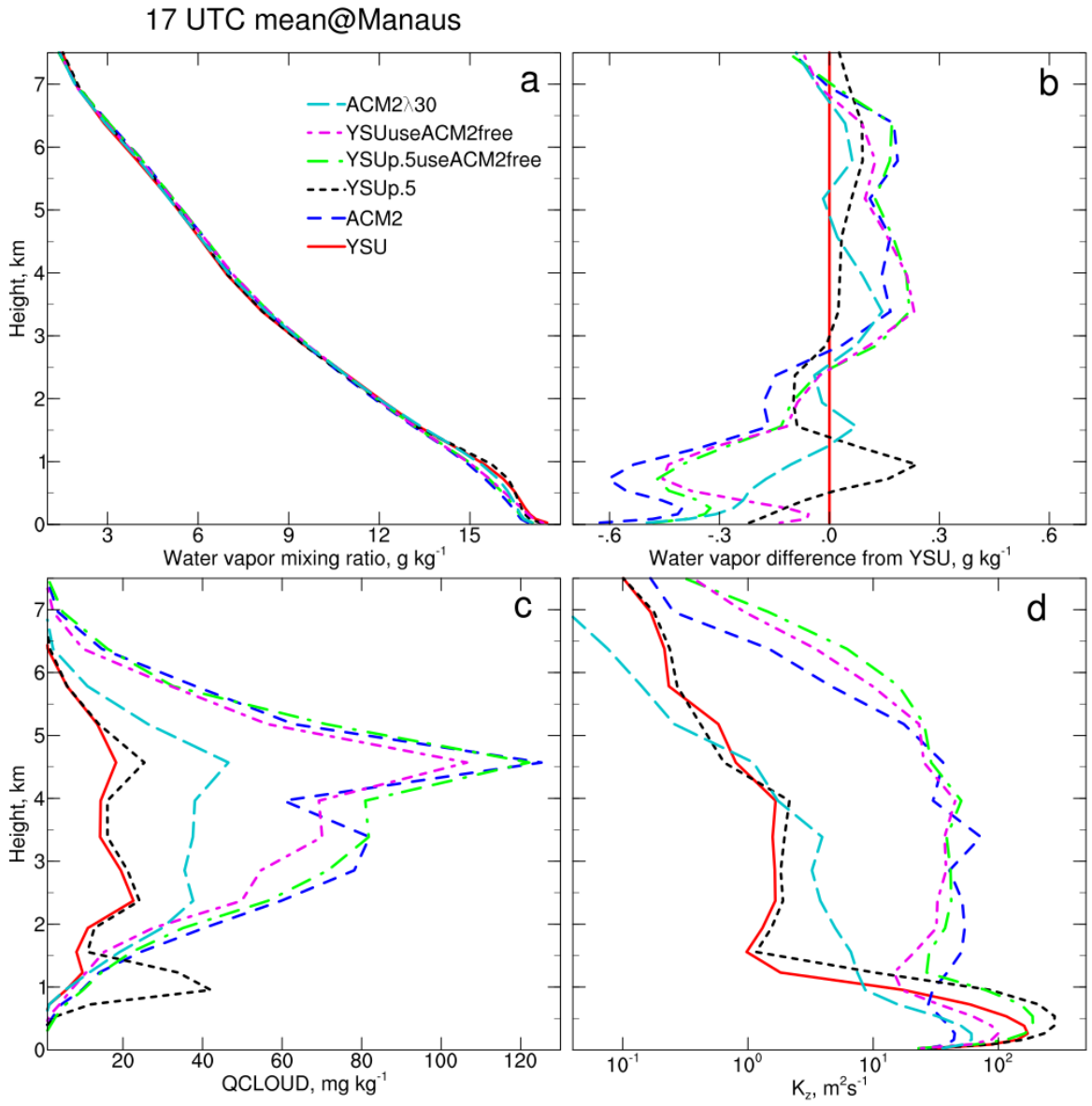

Figure 9. Mean profiles of (a) water vapor mixing ratio, (b) water vapor difference from that simulated by YSU, (c) cloud water mixing ratio (QCLOUD), and (d) vertical mixing coefficient (K_z) at 17 UTC during January-February 2019 at Manaus (location marked in Fig. 8b) simulated by YSU, ACM2 and 4 sensitivity simulations YSUp.5, YSUuseACM2free, YSUp.5useACM2free, ACM2λ30.

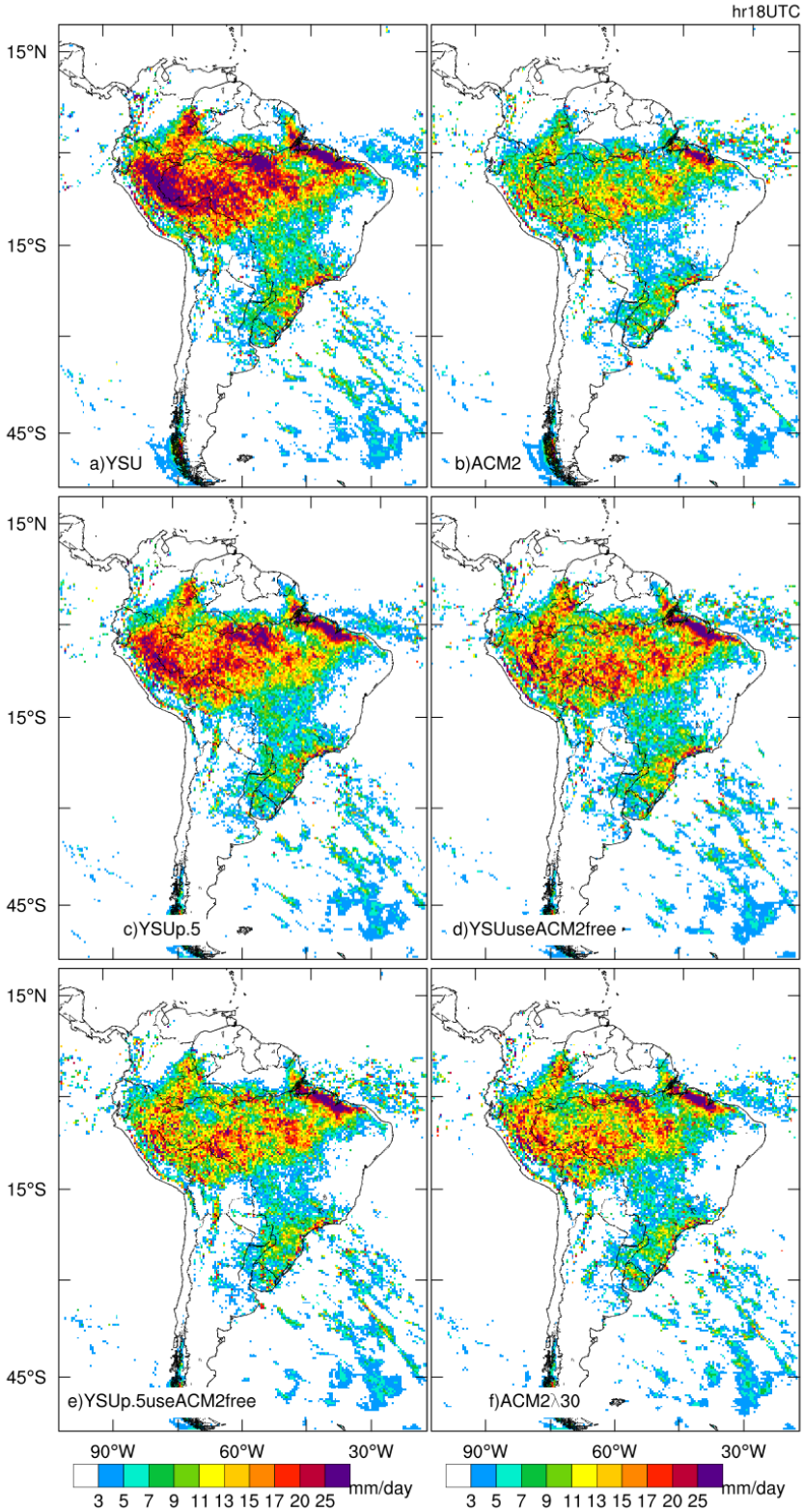

Figure 10. Average precipitation rate at 18 UTC during January-February 2019 simulated by (a) YSU, (b) ACM2 and 4 sensitivity simulations (c) YSUp.5, (d) YSUuseACM2free, (e) YSUp.5useACM2free, (f) ACM2λ30.

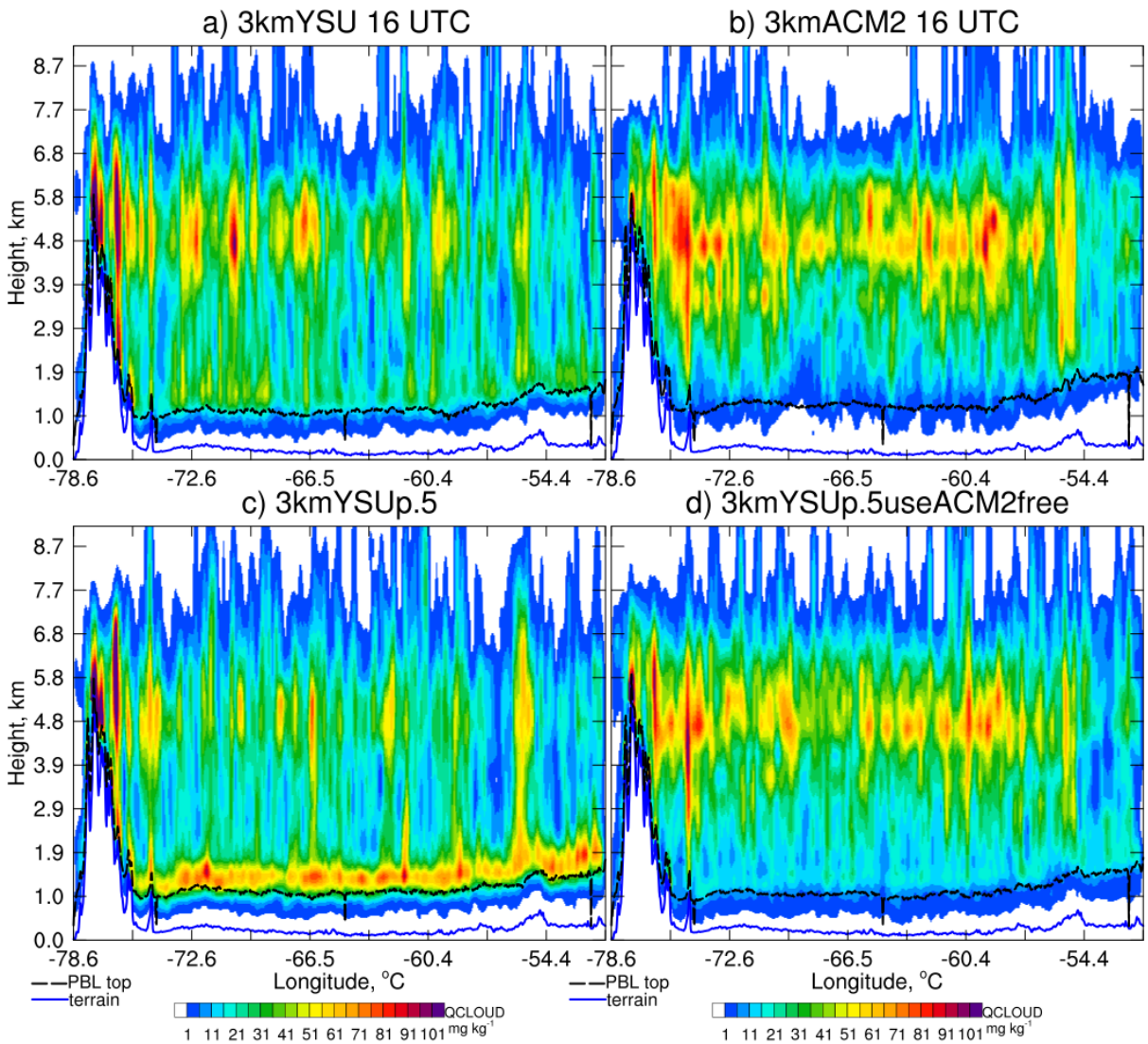

Figure 11. Cross-section of average noon-time cloud water mixing ratios over the Amazon in Jan-Feb 2019 simulated by (a) 3kmYSU , (b) 3kmACM2 , (c) 3kmYSUp. 5 , and (d) 3kmYSUp. 5useACM2free. The location of these cross-sections is marked in Fig. 4l

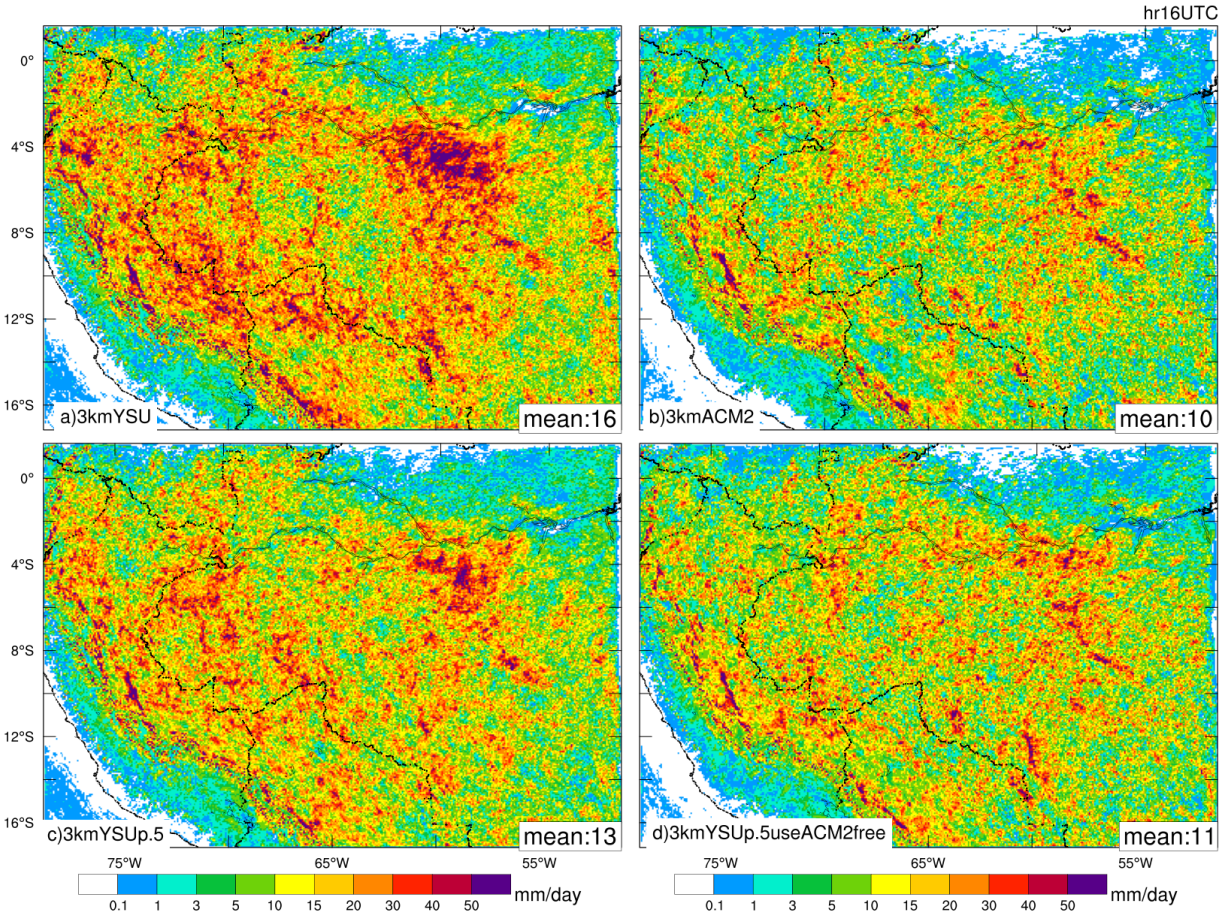

Figure 12. Average noon-time precipitation rate in Jan-Feb 2019 simulated by (a) 3kmYSU, (b) 3kmACM2, (c) 3kmYSUp.5, and (d) 3kmYSUp.5useACM2free. The domain-averaged values are marked.